Zoological Journal of the Linnean Society, 2021, **XX**, 1–39. With 16 figures.

Ontogeny and variation of the pachycephalosaurine dinosaur *Sphaerotholus buchholtzae*, and its systematics within the genus

D. CARY WOODRUFF[1,2,3,*], MARK B. GOODWIN[4], TYLER R. LYSON[5] and DAVID C. EVANS[1,2]

[1]*Royal Ontario Museum, Toronto, ON, CA*
[2]*University of Toronto, Toronto, ON, CA*
[3]*Great Plains Dinosaur Museum, Malta, MT, USA*
[4]*Museum of Paleontology, University of California, Berkeley, CA, USA*
[5]*Department of Earth Sciences, Denver Museum of Nature & Science, Denver, CO, USA*

Received 9 May 2020; revised 19 November 2020; accepted for publication 1 December 2020

The ontogeny and taxonomy of the dome-headed pachycephalosaurs are topics of continued debate. Pachycephalosaurid diversity in the Maastrichtian of North America is particularly controversial, and the validity and composition within the genus *Sphaerotholus* remains unresolved. While the type species, *S. goodwini*, is generally considered valid, debate has centred around the validity and taxonomy of *S. buchholtzae* and *S. edmontonensis*. Here we employ morphometrics, histology and phylogenetic analysis to resolve these issues.

An ontogenetic assessment of *S. buchholtzae* ($N > 20$) confirms previously observed ontogenetic morphologies: inflation of the frontoparietal dome, obliteration of tesserate surface texture, blunting of the peripheral nodes and decreasing void space within the dome. While linear bivariate analysis finds *S. edmontonensis* nested within *S. buchholtzae*, three-dimensional geometric morphometrics supports *S. edmontonensis* and *S. buchholtzae* as distinct species. Phylogenetic analysis recovers a *Sphaerotholus* lineage with *S. goodwini* as sister-taxon to a clade formed by *S. edmontonensis* and *S. buchholtzae*.

The stratigraphic, phylogenetic, morphometric and ontogenetic data support the validity of both *S. edmontonensis* and *S. buchholtzae*, and their placement within the genus *Sphaerotholus*. The morphological similarities of *S. edmontonensis* to immature *S. buchholtzae*, and the slightly older geological age of *S. edmontonensis*, suggest that *S. edmontonensis* and *S. buchholtzae* may be part of an anagenetic lineage.

ADDITIONAL KEYWORDS: pachycephalosaurid – taxonomy – palaeontology – ontogeny.

INTRODUCTION

The Late Cretaceous pachycephalosaurine pachycephalosaurid (Dinosauria: Ornithischia) *Sphaerotholus* Williamson & Carr, 2002 is represented by the genotype *S. goodwini* Williamson & Carr, 2002 from the De-na-zin Member of the Kirtland Formation of New Mexico (73.83 ± 0.18–73.49 ± 0.25 Mya; Fowler, 2017). Several other species from the Campanian–Maastrichtian of the Western Interior variably assigned to this genus, including *S. buchholtzae* Williamson & Carr, 2002 from the Uppermost Hell Creek Formation of Montana and North Dakota (~67.20–66.05 ± 0.008 Mya; Williamson & Carr, 2002; Mallon *et al.*, 2015; Fowler, 2017; Sprain *et al.*, 2018) and *S. edmontonensis* (Brown & Schlaikjer, 1943) from the Tolman Member of Horseshoe Canyon Formation of Alberta, Canada (~68.4–70.9 Mya; Eberth *et al.*, 2013; Mallon *et al.*, 2015; Fowler, 2017). Specimens now assigned to *Foraminacephale brevis* (Lambe, 1918) had also been suggested to be members of *Sphaerotholus* (Longrich *et al.* 2010), but new material and a recent revision of this taxon by Schott & Evans (2016) indicated that *F. brevis* is not closely related to *S. goodwini* and was, therefore, referred to its own genus.

The systematics and taxonomy of the *Sphaerotholus*–*Prenocephale* grade of pachycephalosaurine pachycephalosaurs has remained in flux over the

*Corresponding author. E-mail: sauropod4@gmail.com

past two decades. Numerous studies disagreed on the phylogenetic position and taxonomy of all species that have been referred to *Sphaerotholus*. For example, Sullivan (2000) noted that *S. brevis* and *S. edmontonensis* differed from *Stegoceras* Lambe, 1902 (e.g. Chapman *et al.*, 1981) and recognized both as distinct pachycephalosaurine taxa, referring both species to the Asian genus *Prenocephale* Maryańska & Osmólska, 1974. Williamson & Carr (2002), noted derived traits of the parietosquamosal shelf allied a referred specimen of *P. edmontonensis* (TMP 1987.113.0003) from the Hell Creek Formation of Montana (Giffin, 1989; Sullivan, 2000) with their newly erected *S. goodwini*. They recognized this specimen as the holotype of a second species of *Sphaerotholus*, *S. buchholtzae*, while concurrently considering the holotype of *S. edmontonensis* as non-diagnostic to the genus and species levels. Subsequent studies suggested that *S. edmontonensis* is a valid species of either the genus *Prenocephale* (Sullivan, 2006) or *Sphaerotholus* (Longrich *et al.* 2010; Mallon *et al.*, 2015) or it was tentatively referred to *S. buchholtzae* (e.g. Evans *et al.*, 2013; Williamson & Brusatte, 2016).

The confusion with regards to the systematics of *Sphaerotholus*-like taxa is due, in part, to a lack of specimens and adequate knowledge of ontogeny and variation of the cranial dome in these taxa. Unfortunately, *S. goodwini* and *S. edmontonensis* (*s.s.*, Horseshoe Canyon Formation) are known from no more than three specimens each, most of which are incomplete and poorly preserved (Sullivan, 2000, 2006; Williamson & Brusatte, 2016). Conversely, *S. buchholtzae* from the extensively studied Hell Creek Formation (Hartman *et al.*, 2002 GSA Sp. Vol. 361; Wilson *et al.*, 2014 GSA Sp. Paper 503 and references therein) and its equivalents (e.g. Mallon *et al.*, 2015), is known from over 20 cranial specimens that represent a significant size range and form a hypothesized ontogenetic series. The ontogenetic development of *S. buchholtzae* has never been previously examined, despite the availability of a relatively large sample set. Many of the specimens include parietosquamosal ornamentation that allows an assessment of intraspecific variation in this phylogenetically important region of the skull for the first time.

Here we adopt a multiproxy approach to examine variation in *S. buchholtzae* following the schema of Schott *et al.* (2011) and Schott & Evans (2016), using morphometrics, histology and phylogenetic analysis, in a biostratigraphic context. This study provides a framework for testing hypotheses on the taxonomic validity and relationships of species within *Sphaerotholus* and closely related taxa, and contributes to a better understanding of pachycephalosaurid diversity in the latest Cretaceous of North America.

MATERIAL AND METHODS

All specimens were macroscopically examined to note relative size, proportions, frontoparietal dome and parietosquamosal node morphology, among other traits. We presumed that relative size correlated with ontogeny (smaller = younger, larger = older; Fig. 1). Any observable size-related trends or patterns were subsequently evaluated using histological relative-age assessment and stratigraphic positioning to determine relative ontogeny. Most measurements were taken using standard digital callipers. Those measurements not possible to record due to the length or orientation of the external jaws, such as the depth from the endocranial fossa to the apex of the dome, were calculated using digital iGaging outside digital calipers. A list of all specimens included in this analysis and their provenance is provided in Table 1.

Horner & Goodwin (2009) used Computed Tomography (CT) and cranial histology to assess cranial tissues and the ontogenetic status of *Pachycephalosaurus* Brown & Schlaikjer, 1943. Schott *et al.* (2011) and Schott & Evans (2016) tested hypothesized ontogenetic series of pachycephalosaurid domes using high-resolution X-ray computed tomography (HRCT). For this analysis, three *S. buchholtzae* specimens that encompass the known size range of domes from the Hell Creek Formation were scanned by standard clinical CT, microtomography (MicroCT) and HRCT: UCMP 186026 is the smallest dome with a frontoparietal (fp) length = 75.94 mm; DMNH EPV.97077 is the largest specimen with a fp length = 113.84 mm; and UWBM 89701 falls in-between these two with a fp length = 96.78 mm; ROM 53584, one of the largest specimens in the *Sphaerotholus* dataset (fp = 111.75 mm), was HRCT scanned at the University of Texas, Austin, but artefacts and noise distortion prevented microstructural analysis. Scan specifications for each specimen are provided in Supporting Information, File S1. Following Schott *et al.* (2011): (1) coronal scan sections were taken at a homologous location in all three specimens at the contact between the posterior supraorbital and postorbital sutures, and (2) an area was defined from the top of the endocranium to the dorsal edge of the frontal and laterally to the edge of the dome. Relative void space was calculated using the Huang method (Huang & Wang, 1995; Wang *et al.*, 2002) in ImageJ (Abramoff *et al.*, 2004) for each homologous region. From these threshold images, the voxel counter plug-in was used to quantify void space, a proxy for relative vascularity of the dome (see: Schott *et al.*, 2011; Horner & Goodwin, 2009). The per cent void space was then correlated to the relative size of specimens to test the proposed ontogenetic sequence.

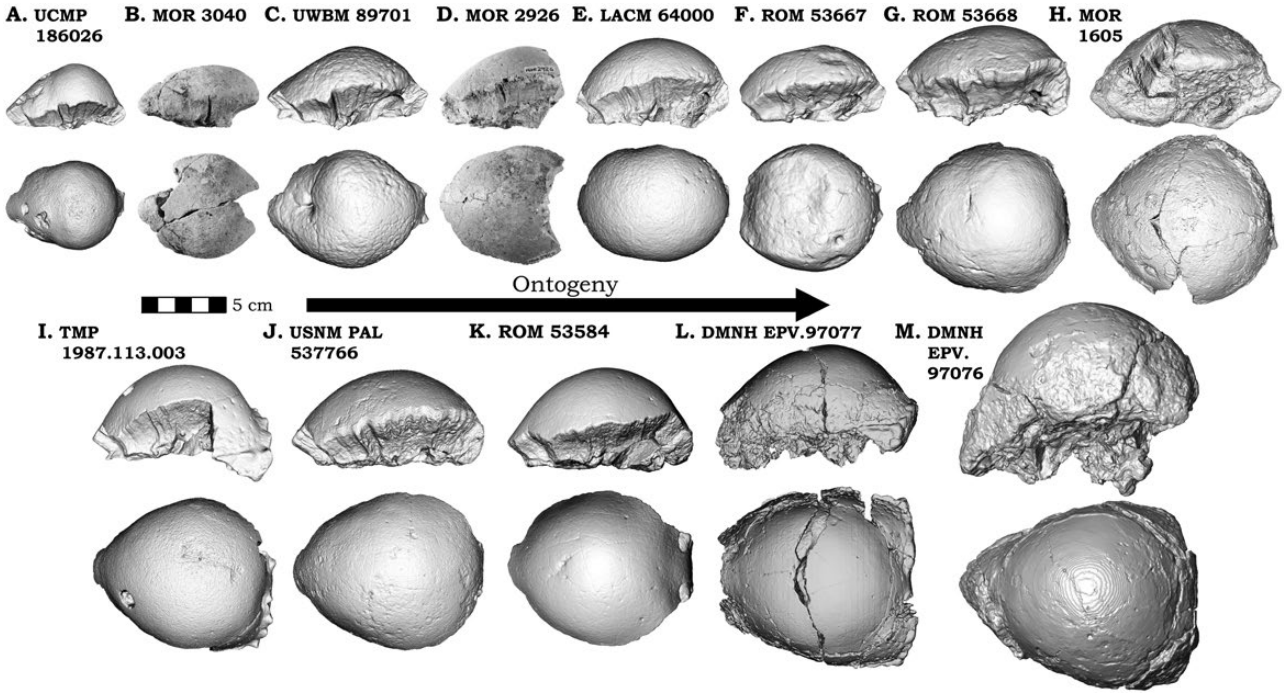

Figure 1. *Sphaerotholus buchholtzae* specimens examined in this analysis in left lateral and dorsal orientations. Specimens ranked in hypothesized ontogenetic order. All specimens to scale. Top row (left to right): A, UCMP 186026; B, MOR 3040; C, UWBM 89701; D, MOR 2926; E, LACM 64000; F, ROM 53667; G, ROM 53668. Bottom row (left to right): F, ROM 53667; G, ROM 53668; H, MOR 1605; I, TMP 1987.113.0003; J, USNM PAL 537766; K, ROM 53584; K, ROM 53584; L, DMNH EPV.97077; M, DMNH EPV.97076. All specimens to scale. Scale bar = 5 cm.

Morphometrics

The complex cranial morphology expressed during ontogeny was quantified using several morphometric approaches utilized successfully in previous studies (Schott *et al.*, 2011; Schott & Evans 2016; Williamson & Brusatte, 2016). Since these frontoparietal domes represent complex ovoid structures, the differences between species may be subtle. As a result, we tried to capture several degrees of complexity. Traditional linear measurements based on landmark data (e.g. Goodwin, 1990) have been employed in bivariate analyses that compare two linear variables (such as length versus width) in multiple pachycephalosaurid studies (e.g. Chapman *et al.*, 1981; Schott *et al.*, 2011; Evans *et al.*, 2013; Schott & Evans, 2016), as well as in multivariate analyses (Chapman *et al.*, 1981; Mallon *et al.*, 2015; Williamson & Brusatte, 2016). Alternatively, landmark-based geometric morphometrics (GM) allow for a more accurate description of the spatial geometry of the specimen, because the landmarks remain ordinated in space. Multiple and easily identified homologues landmarks on pachycephalosaurid frontoparietal domes (Goodwin, 1990), contribute to their suitability in GM studies. Two-dimensional (2D) landmark-based GM uses homologous points to construct orthogonal transformations, reflecting the degree of variance (a.k.a. principal component analysis; PCA). While 2D PCAs are valuable for determining the variation of structures as a whole, they still only reflect a single anatomical orientation at a time. The compression of spatial data is potentially problematic in three-dimensional structures, such as pachycephalosaurid frontoparietal domes. We employed three-dimensional (3D) landmark-based GM in order to more accurately capture the complexities and anatomical nuances of the frontoparietal domes. This 3D-based method reflects the entire structure, is more inclusive and allows for direct specimen-level geometry-based comparisons, compared to variable comparisons (using length, width or height). We compared these different methods to capture the range of morphological complexity in these pachycephalosaurid domes. Only one *S. buchholtzae* specimen (UWBM 89701) was excluded from the 3D GM analysis due to severe pathology on one side of the dome, but was included in the remaining analyses.

Each specimen was measured using the techniques outlined above for the linear bivariate plots and the logged value variables were graphed in Microsoft Excel. Three variables were analysed and compared to a standard variable of frontoparietal length (dome thickness, greatest width, length of postorbital), in addition to a comparison of frontal-to-parietal lengths.

Table 1. Database of known *Sphaerotholus* specimens. Species-level designations primarily follow previous identifications. FP = frontoparietal; NA = not applicable

Specimen	Species	Formation	Location	Completeness	FP Length	Reference
AMNH FARB 30044	*S. buchholtzae*	Hell Creek Fm.	Wibaux Co. Montana	A complete frontoparietal dome	74.47 mm	Peterson *et al.*, 2013.
CMN 56510	*S. buchholtzae*	Frenchmen Fm.	Saskatchewan, Canada	An isolated left postorbital	NA	Mallon *et al.*, 2015.
DDM 1567.18	*S. buchholtzae*	Hell Creek Fm.	Carter Co., Montana	An isolated left squamosal	NA	——
DMNH EPV.97077	*S. buchholtzae*	Hell Creek Fm.	Bowman Co., North Dakota	A complete frontoparietal dome with all peripheral elements	118.09 mm	Bourke *et al.*, 2014.
DMNH EPV.97076	*S. buchholtzae*	Hell Creek Fm.	Slope, North Dakota	A complete frontoparietal dome	NA	Bourke *et al.*, 2014.
DMNH EPV.97078	*S. buchholtzae*	Hell Creek Fm.	Slope, North Dakota	Partial nasals	NA	Bourke *et al.*, 2014.
LACM 15345	*S. buchholtzae*	Hell Creek Fm.	Garfield Co., Montana	A heavily weathered frontoparietal dome	NA	——
LACM 64000	*S. buchholtzae*	Hell Creek Fm.	Garfield Co., Montana	A complete frontoparietal dome	90.47 mm	Goodwin, 1990.
MOR 1605	*S. buchholtzae*	Hell Creek Fm.	Garfield Co., Montana	A heavily weathered frontoparietal dome	113.48 mm	——
MOR 2926	*S. buchholtzae*	Hell Creek Fm.	Garfield Co., Montana	The anterior ~2/3 of the frontopairetal dome	74.69 mm (incomplete)	——
MOR 3040	*S. buchholtzae*	Hell Creek Fm.	Garfield Co., Montana	A weathered frontoparietal dome	76.26 mm (damaged)	——
ROM 53582	*S. buchholtzae*	Hell Creek Fm.	Garfield Co., Montana	An isolated right squamosal	NA	——
ROM 53584	*S. buchholtzae*	Hell Creek Fm.	Garfield Co., Montana	A complete frontoparietal dome	111.75 mm	——
ROM 53585	*S. buchholtzae*	Hell Creek Fm.	Garfield Co., Montana	A heavily weathered frontoparietal dome	97.66 (damaged)	——
ROM 53667	*S. buchholtzae*	Hell Creek Fm.	Garfield Co., Montana	A nearly complete frontoparietal dome with a large pathology over the majority of the dome	NA	——
ROM 53668	*S. buchholtzae*	Hell Creek Fm.	Fallon Co., Montana	A nearly complete frontoparietal dome	104.47 mm	——
ROM 64809	*S. buchholtzae*	Hell Creek Fm.	Garfield Co., Montana	An isolated right squamosal	NA	——
ROM 75853	*S. buchholtzae*	Hell Creek Fm.	Harding Co., South Dakota	A highly fragmentary specimen that preserves the squamosals and right post orbital	NA	——
TMP 1987.113.0003	*S. buchholtzae*	Hell Creek Fm.	Carter Co., Montana	A complete frontoparietal dome with left squamosal	112.27 mm	Williamson & Carr, 2002.
UCMP 186026	*S. buchholtzae*	Hell Creek Fm.	Garfield Co., Montana	A complete frontoparietal dome	75.94 mm	——
USNM PAL 537766	*S. buchholtzae*	Hell Creek Fm.	Garfield Co., Montana	A complete frontoparietal dome	116.15 mm	——

Table 1. Continued

Specimen	Species	Formation	Location	Completeness	FP Length	Reference
UWBM VP 89701	*S. buchholtzae*	Hell Creek Fm.	Garfield Co., Montana	A complete frontoparietal dome	96.78 mm	——
UWBM VP 119701	*S. buchholtzae*	Hell Creek Fm.	Garfield Co., Montana	A complete frontoparietal dome	129.91 mm	——
NMMNH P-27403	*S. goodwini*	De-na-zin Mbr. Kirtland Fm.	San Juan Co., New Mexico	A complete frontopairetal dome with right squamosal and incomplete basicranium	130.5 mm	Williamson & Carr, 2002.
NMMNH P-30068	*S. goodwini*	Farmington Mbr. Kirtland Fm.	San Juan Co., New Mexico	Fragmentary left squamosal and left dentary.	NA	Williamson & Carr, 2002.
SMP VP-1084	*S. goodwini*	De-na-zin Mbr. Kirtland Fm.	San Juan Co., New Mexico	A heavily weathered frontoparietal dome	NA	Williamson & Brusatte, 2016.
NMMNH P-41020	*S. goodwini*	De-na-zin Mbr. Kirtland Fm.	San Juan Co., New Mexico	NA	NA	Williamson & Brusatte, 2016.
NMMNH P-41125	*S. goodwini*	De-na-zin Mbr. Kirtland Fm.	San Juan Co., New Mexico	NA	NA	Williamson & Brusatte, 2016.
CMN 8830	*S. edmontonensis*	Edmonton Fm.	Alberta, Canada	A heavily weathered frontoparietal dome	92.88 mm	Williamson & Carr, 2002.
CMN 8831	*S. edmontonensis*	Edmonton Fm.	Alberta, Canada	A heavily weathered frontoparietal dome	NA	Williamson & Carr, 2002.
CMN 8832	*S. edmontonensis*	Edmonton Fm.	Alberta, Canada	Heavily weathered anterior ~half of the frontoparietal dome	NA	Williamson & Carr, 2002.

The GM techniques 'raw data' consisted of 3D models of each specimen. All but one of the 3D models (DMNH EPV.97077 via microtomography) were constructed via photogrammetry, following Falkingham (2012) and Mallison & Wings (2014). Photogrammetric processing used Agisoft PhotScan v.1.2.6 build 2834 software. Once the photogrammetric models were constructed, for 2D GM, the models were oriented in a standard anatomical orientation, and homologous landmarks were placed on each image (Fig. 2). Next, the landmarked images were uploaded into Comprehensive R Archive Network, CRAN (R Development Core Team, 2008) v.3.3.2. Principal component analyses (PCA) were constructed using the GM shape analysis package GEOMORPH (Adams & Otárola-Castillo, 2013). For 3D GM, the 3D model files were uploaded into the Institute for Data Analysis and Visualization's program LANDMARK 3.6 (Wiley *et al.*, 2005). As in the 2D GM, the 3D landmarked images and the resulting PCA were uploaded and constructed in R using the GEOMORPH package (R Development Core Team, 2008; Adams & Otárola-Castillo, 2013). Due to incomplete specimens in both the 2D and 3D analyses, we opted to estimate for missing landmarks using the estimate.missing function in R (Adams & Otárola-Castillo, 2013). There are certainly negatives of estimating landmarks; mainly it could be assigning an inaccurate spatial location, and with more specimens that are spatially similar, the missing landmarks will be more heavily estimated towards the dominating mean. Three-dimensional graphical reconstructions were produced in JMP,1989–2019. The first two PC axes were correlated with the log of frontoparietal length, a proxy of size, to assess for possible allometry.

It is important to note that DMNH EPV.97076, DMNH EPV.97077 and DMNH EPV.97078 represent among the largest and most complete *S. buchholtzae* specimens yet known. While these specimens were CT-scanned, the quality of the scan data, plus taphonomic damage/distortion, do not allow them to be segmented, measured (i.e. peripheral element measurements), nor accurately position landmarks in all three geometric morphometric analyses. These specimens were not included in morphological analyses that focus on isolated frontoparietal domes, but they were included in our anatomical descriptions, and DMNH EPV.97077 serves as a maturational endmember.

Phylogenetic analysis

Parsimony and Bayesian phylogenetic analyses were conducted on a modified version of the Pachycephalosauria matrix of f Evans *et al.* (2013) consisting of 51 characters and 21 in group taxa (see Appendix I for character states and matrix). The ceratopsian taxa *Yinlong downsi* Xu *et al.*, 2006 and *Psittacosaurus mongoliensis* Osborn, 1923 were used as outgroup taxa. For the parsimony analysis, the matrix was analysed in PAUP* v.4.0a157 (Swofford, 2002) with the maximum parsimony criterion and the branch-and-bound search algorithm, and a bootstrap analysis of 10 000 replicates was conducted to assess the robustness of the hypothesis. While maximum parsimony is currently the standard method used for palaeontological datasets, Bayesian methods have recently been argued to produce a more accurate resolution (Wright & Hillis, 2014; O'Reilly *et al.*, 2016; Puttick *et al.*, 2017). To compare the robustness of the data to different search algorithms, we analysed the matrix with both methods (e.g. Brooks *et al.*, 2007). Bayesian analyses were run in MrBayes v.3.2.6 (Ronquist *et al.*, 2012). We ran the analysis for 2 million generations (four chains, two runs) with a sampling frequency of 1000 for each dataset. Priors were kept to standard settings. The trees generated during the first 10 000 generations were discarded as burn-in for the compilation of the majority-rule consensus tree. Clade credibility values were then calculated, with values greater than, or equal to, 70% considered highly supported (Heled & Bouckaert, 2013).

Phylogenetic definitions

We follow the phylogenetic definition of Pachycephalosauridae established by Sereno (1997) as the least inclusive clade containing *Stegoceras validum* (Lambe, 1918) and *Pachycephalosaurus wyomingensis* (Gilmore, 1931). Additionally, we follow the well-established and widely used definition of Pachycephalosaurinae, first provided by Sereno (1998) as a stem-based clade to include pachycephalosaurs more derived than *Stegoceras validum*, and restated by Sereno (2005) as 'the most inclusive clade containing *Pachycephalosaurus wyomingensis* Gilmore 1932 but not *Stegoceras validum* Lambe 1918'.

Institutional abbreviations

AMNH FARB, American Museum of Natural History, New York, NY, USA; CMN, Canadian Museum of Nature, Ottawa, ON, Canada; DDM, Dinosaur Discovery Museum, Kenosha, WI, USA; DMNS, Denver Museum of Nature & Science, Denver, CO, USA; LACM, Los Angeles County Museum, Los Angeles, CA, USA; MOR, Museum of the Rockies, Bozeman, MT, USA; SMP, State Museum of Pennsylvania, Harrisburg, PA, USA; ROM, Royal Ontario Museum, Toronto, ON, Canada; TMP, Royal Tyrrell Museum of Palaeontology, Drumheller, AB, Canada; UCMP, University of California Museum of Paleontology, Berkeley, CA, USA; USNM, United States National Museum, Washington, DC, USA; UWBM, University of Washington Burke Museum, Seattle, WA, USA; Z. Pal, Palaeozoological Institute, Polish Academy of Sciences, Warsaw, Poland.

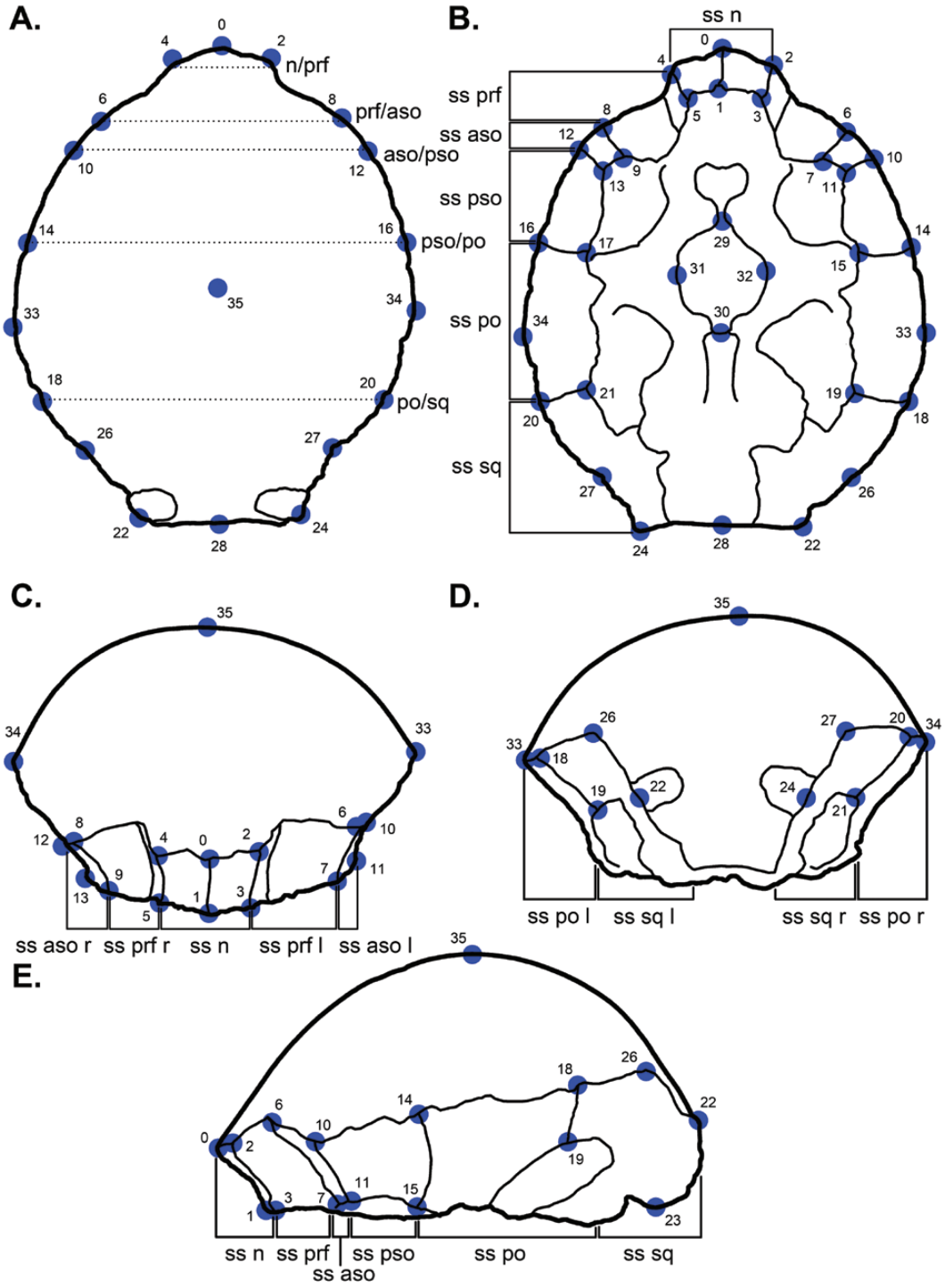

Figure 2. Schematic diagram of *Sphaerotholus buchholtzae* (ROM 53584) in dorsal (A), ventral (B), anterior (C), posterior (D) and left lateral (E) orientation. Blue dots and numbers correspond to landmarks used in both 2D and 3D GM analyses. All orientations to scale. Abbreviations: ss, sutural surface; l, left; r, right; aso, anterior supraorbital; n, nasal; prf, prefrontal; po, postorbital; pso, posterior supraorbital; sq, squamosal.

RESULTS

Morphological description

We examined 22 known *S. buchholtzae* specimens consisting of partial to complete frontoparietals, as well as several isolated squamosals (Table 1). UCMP 186026, UWBM 89701, ROM 53584 and DMNH EPV.97077 (see Fig. 3) encompass the known size range, in ascending order from smallest to largest. These specimens were also CT-scanned to confirm relative vascularity and histological details (see Supporting Information for specimen scan specifications).

UCMP 186026

UCMP 186026 is a complete, well-preserved frontoparietal dome and the smallest specimen in the sample set assigned to *S. buchholtzae*, with a frontoparietal length of 75.94 mm (Fig. 3). Contact surfaces for the adjoining peripheral elements are preserved. The dome is ovoid in dorsal view, laterally widest posteriorly and the rectangular nasal process of the frontals contributes to about 17% of the total length. The angle of the prefrontal–frontal contact relative to the midline is approximately 128° dorsally. The parietal appears 'bulbous' and the orientation of the frontoparietal–squamosal contact relative to the midline is 150–162°. The external surface of the frontoparietal is covered by a tesserate texture that is prominent around the periphery, only faintly developed at the apex and typically associated with immature specimens of *Stegoceras validum* (Williamson & Carr 2002; Goodwin & Horner 2004; Schott *et al.*, 2011) and *Colepiocephale lambei* (Sternberg, 1945) (Schott *et al.*, 2009) with incomplete expansion of the frontoparietal dome. Near the frontal–parietal contact there is a slight depression on the dome surface adjacent to the dorsal contact of the postorbital and posterior supraorbital, also present in *Colepiocephale* (Schott *et al.*, 2009) and *Stegoceras* (Schott *et al.*, 2011), but absent in larger, more mature, specimens. There are approximately 20 foramina distributed over the posterior portion of the parietal, concentrated peripherally and similar to the pattern observed in *Foraminacephale* (Schott & Evans, 2016). The majority of the foramina are clustered close to the parietal–squamosal contact, and are staggered or subequal in distance to one another. A minimum of three concave lesions (pathologies) occur on the left portion of the anterodorsal surface of the frontal.

In lateral view, the apex of the dome has an asymmetric profile. The posterior region of the frontoparietal dome is inflated more than the anterior portion. The dorsal margin of the frontals is sloped 40° from the horizontal to the dome apex, which occurs on the midline, slightly posterior to the frontoparietal contact (this contact is seen ventrally in the endocranial fossa). Anterior to the apex of the dome, a small, transverse depression along the frontal–parietal suture, suggests independent doming of the constituent bones (as in *S. validum*; Schott *et al.*, 2011). The anterior supraorbital contact is a thin slip compared to that of the posterior supraorbital, and the dorsal margins of the posterior supraorbital contact and the postorbital contact are basically continuous. Along with the overall 'bulbous' morphology of the posterior region of the frontoparietal, the lateral surfaces near the apex of the dome are subtly inflated with a slight depression down the midline. Posteriorly, the parietal is steeply sloped (~54°) in the last third of the dome. The posteriormost portion of the parietals and the anteriormost portion of the frontals are nearly on the same plane and of similar dimensions (dorsovental height vs. anteroposterior length), yet the frontals' anterior projection is longer that the posterior intersquamosal process of the parietal. The supratemporal fenestra are closed. The dorsoventral thickness of the dome at the contact point between the squamosal, postorbital and parietal is 8.02 mm. The temporal chamber is less developed compared to that of more mature specimens and the chamber roof is subhorizontal, unlike the vaulted condition in larger and presumably older individuals.

In lateral view, there is a gentle inflection of the dorsal margin between the dome apex and the posterior parietal projection. In dorsal, posterior and ventral views, this posterior parietal bridge has a convex or saddle-shaped morphology. This posterior bridge is 11.62 mm wide across the base of the primary node row and contributes to the relatively wide surface of the parietosquamosal bar in posterior view. The articulation/indentation for the parietosquamosal nodes is evident at the parietal–squamosal contact. Only half of the right node is present, whereas the left is absent, demonstrating asymmetry in the expression of the nodes on the posterior intersquamosal portion of the parietal (see below). The preserved right node appears to be generally flattened with a slightly raised midpoint.

In ventral view, the morphology is less consistent less consistent with the larger *S. buchholtzae* specimens in the series (see below and Supporting Information), suggestive of some degree of brain allometry through ontogeny (*sensu* Bhullar *et al.*, 2012; Lautenschlager & Hübner, 2013; Kawabe *et al.*, 2015). The cerebral fossa is circular and approximately 89% laterally wide as anteroposteriorly long. The cerebral fossa is approximately 60% of the total endocranial fossa anteroposterior length, and is anteroposteriorly longer than laterally wide. The anteriormost 66% of the endocranial fossa is on the frontal, and a laterally transecting suture between the frontals and parietals is clearly evident. The olfactory bulbs are prominent,

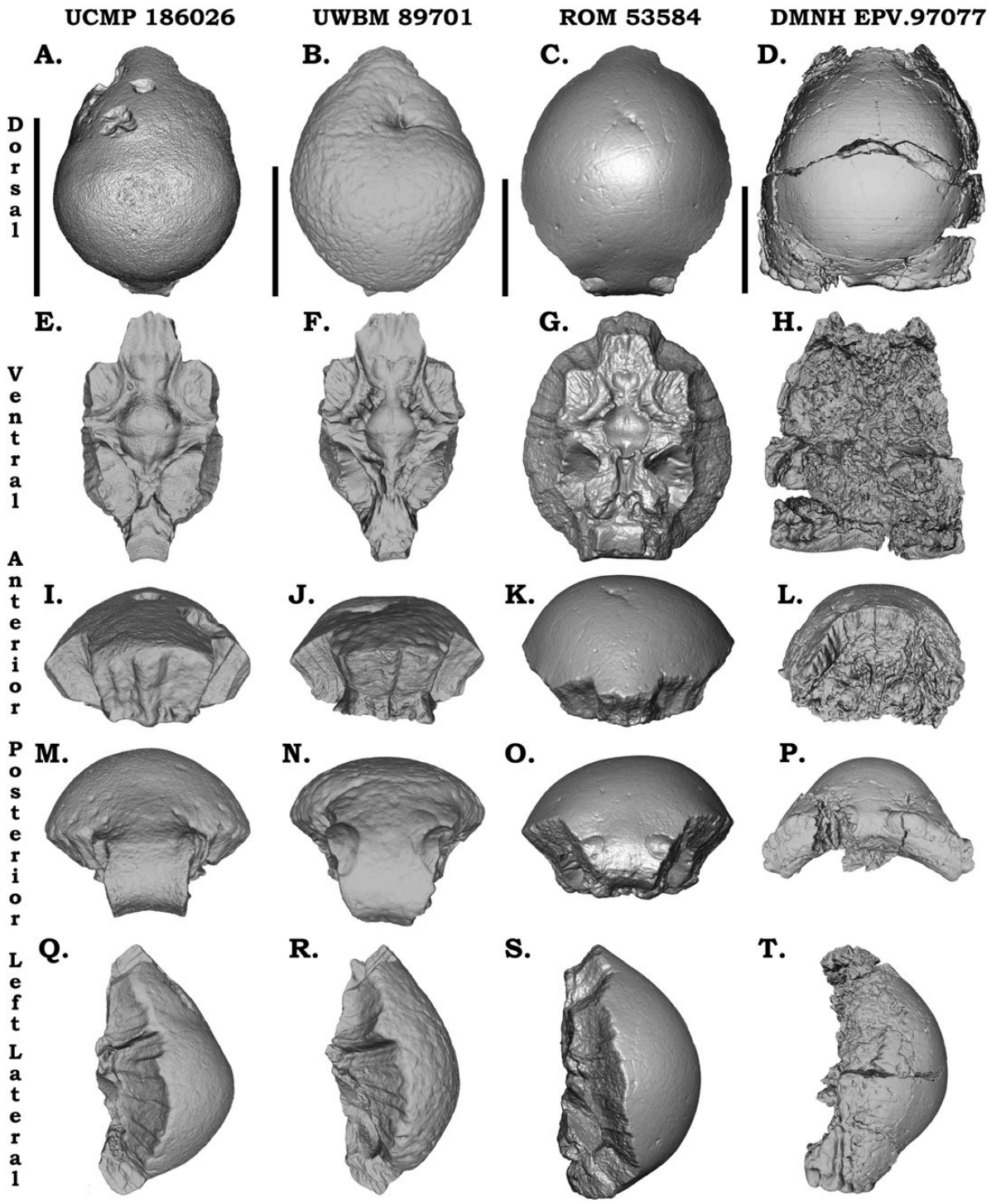

Figure 3. *Sphaerotholus buchholtzae* specimens that span the ontogenetic series, and were the primary specimens examined in this study: UCMP 186026 (A, E, I, M, Q), UWBM 89701 (B, F, J, N, R), ROM 53584 (C, G, K, O, S), DMNH EPV.97077 (D, H, L, P, T). Specimens in dorsal, ventral, anterior, posterior and left lateral orientation (from top to bottom). Specimens not to scale. Scale bars = 5 cm.

but unlike *Stegoceras* and *Colepiocephale* (Schott *et al.*, 2009), where the olfactory bulbs emarginate and are approximately equivalent to the cerebral fossa in size, the bulbs of UCMP 186026 are more coalesced and are approximately 34% the anteroposterior length and 57% the lateral width of the cerebral fossa.

UWBM 89701

UWBM 89701 is ~1.08 times longer than ROM 53586. Based on its overall morphology, this specimen represents a slightly more immature individual (Fig. 3). A large lesion on the frontal distorts the right lateral profile of the dome. In left lateral view, the profile is reminiscent of ROM 53614 with a low angled anterior portion climbing to the dome apex, but in right lateral view, it is distorted by a convex kink leading to the dome apex due to the lesion and modified surrounding tissue. The tesserae texture covers the entire dorsal surface of the dome. The grooves – or sulci – near the presumed frontal–parietal junction observed in ROM 53586 may be present, but the large lesion affects the whole of the frontal curvature. In dorsal view, the anteriormost frontals (measured from the visible suture on the endocranial fossa, since it is obliterated in lateral and dorsal views) constitute approximately 18% of the total length. This is proportionally greater than ROM 53586. In dorsal view, the angle of the prefrontal–frontal contact is approximately 140–149°. The parietals are dorsoventrally inflated but posteriorly, the apex of the dome appears slightly flattened. In right lateral view, on the anterior side, a slope of 33° to the dome apex is likely altered by the frontal lesion. The posterior region of the frontoparietal has a slope of 45°. In the posteriormost 20.4 mm of the frontoparietal, the curvature of the dome decreases and terminates into the posterior parietal processes. Approximately a dozen foramina on the posterior portion of the parietals are visible on the slightly weathered surface of the dome. Due to this weathering, an exact count is not possible. These foramina are subequally spaced, not present along the midline in UWBM 89701, as well as UCMP 186026 and ROM 53586, and are less confined dorsally compared to ROM 53586.

The anteriormost frontal process and the posteriormost parietal process are in the same plane. However, in UWBM 89701 the maximum dorsoventral thickness of the parietal is slightly higher than that of the frontal projection. The frontal and parietal are anteroposteriorly elongate, yet these projections are nearly equal in ROM 53614. In dorsal, posterior and ventral views, this anterioposteriorly short parietal projection of UWBM 89701 has a gentle convex or saddle-shaped morphology similar to that observed in ROM 53586.

Along the parietal–squamosal contact, the articulation/indentation for the contacting parietosquamosal nodes are both present. Half of the left and a third of the right nodes are present. The more complete left node is conical with a more uniform pointed core. In dorsal view, the angle between the parietal–squamosal articulations varies between 144° and 165°. In dorsal view, the dome profile is ovoid with the lateral margins of the parietals contributing to the widest margin, producing an egg-shaped profile (also exhibited by ROM 53614). The apex of the dome is slightly posterior on the frontoparietal. Based on the angle of the anterior region of the frontoparietal, the subequal frontal and parietal lengths calculated from the ventral frontoparietal suture and the egg-shaped dorsal profile, the overall morphology of the dome closely resembles ROM 53614, supporting a slightly more immature age assignment than ROM 53586.

In ventral view, the overall morphology of this specimen is consistent with that of *Colepiocephale* (Schott *et al.*, 2009) and *Foraminacephale* (Schott & Evans, 2016). The endocranial fossa is ovoid, being approximately 1.4 times anteroposteriorly longer than laterally wide. The cerebral fossa is approximately 63% the total endocranial fossa anteroposterior length, and is ovoid in shape, being anteroposteriorly longer than laterally wide. The anteriormost 57% of the endocranial fossa is on the frontal, and a laterally transecting suture between the frontals and parietals is evident. The olfactory bulb fossae are similar in shape to that of *Stegoceras* and *Colepiocephale* (Schott *et al.*, 2009), where the olfactory bulbs anterolaterally diverge and are equivalent to the cerebral fossa in area.

ROM 53584

ROM 53584 is the penultimate dome in the series. There is a single, deep lesion along the midline, along the frontal–parietal contact. In dorsal view, the angle of the prefrontal–frontal contact is approximately 149–155°. The dome has a uniform curvature with little differentiation between the frontals and parietal dorsally. In lateral view, there is a slope of 45° to the dome apex anteriorly. Moving posteriorly along the curvature of the dome, there is a slope of 50°. In the posteriormost ~17 mm of the parietal dome curvature, it quickly and suddenly drops to the posteriormost parietal processes. A few foramina are infrequently dispersed across the entire dome, but the surface texture is nearly uniformly smooth. The anteriormost frontal process and the parietal posteriormost process are approximately on the same plane. The dorsoventral height of the frontal projection is slightly greater than that of the parietal projection. However, the lengths of the frontal and parietal projections are very close (12.7% for the frontal projection and 19.6% for the parietal projection). The posterior parietal projection is anteroposteriorly short, yet extremely wide, producing a laterally elongate, rectangular-shaped process. Also, posteriorly from the frontoparietal dome curvature, there is a sudden transition to this posterior process. This transition is abrupt, and this transitional area

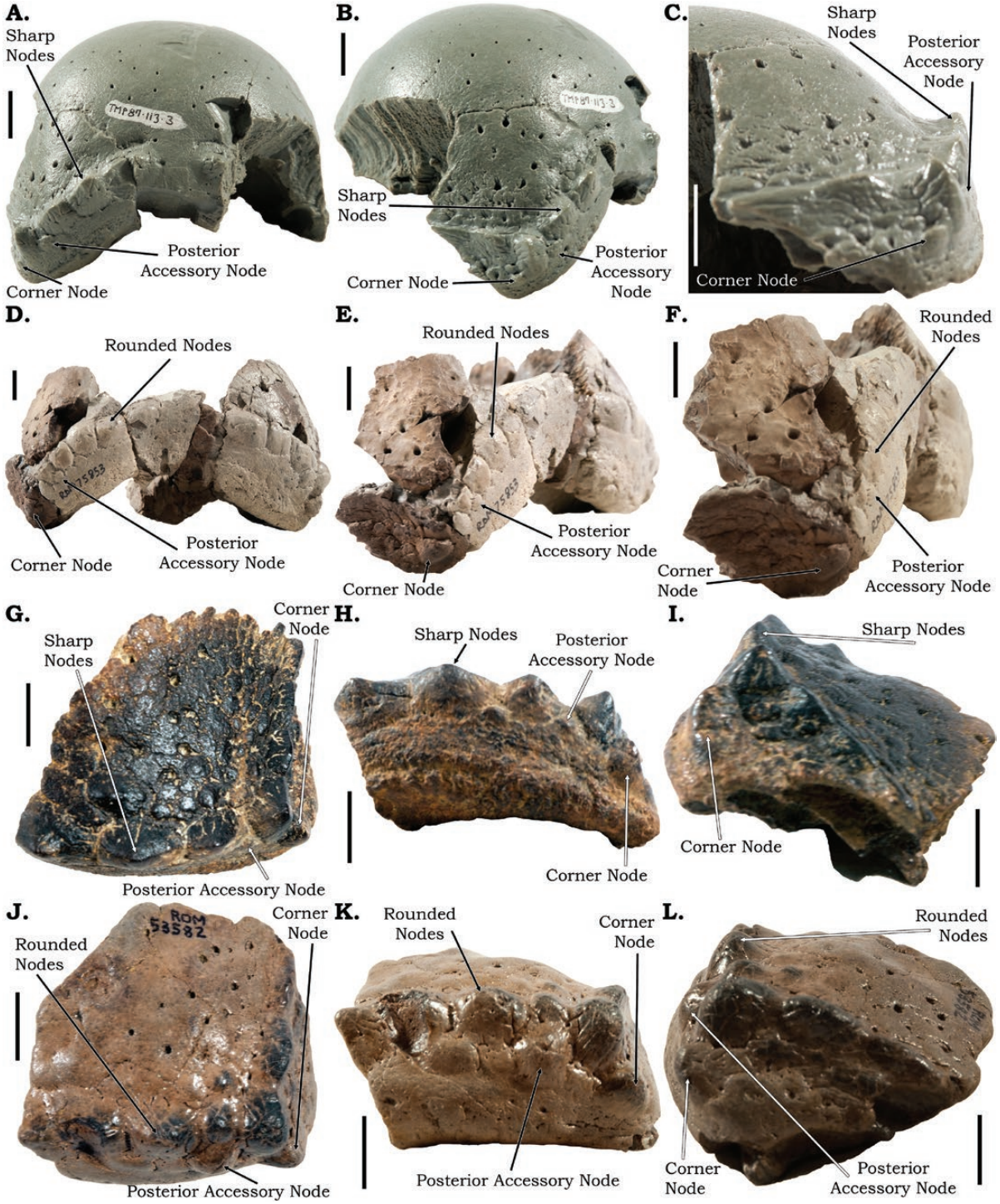

Figure 4. Squamosals from select *S. buchholtzae* specimens highlighting some of the observed patterns of variation and the ontogenetic development. A–C, TMP 1987.113.0003 in posterior (A), left posterolateral oblique (B) and left lateral (C) views. D–F, ROM 75835 in posterior (A), dorso- left posterolateral (B) and left posterolateral (C) views. G–I, ROM in dorsal oblique (A), posterior ventral (B) and right lateral oblique (C) views. J–L, ROM 53582 in dorsal oblique (A), posterior ventral (B), and right lateral oblique (C) views. Specimens not to scale. Scale bars = 1 cm.

of the dome is practically flat (this flat area is also observed laterally in posterior view). Dorsoventrally, the posterior parietal process is gently convex or saddle-shaped. At the parietal–squamosal contact, parietosquamosal nodes are partially preserved and circular to ovoid in overall appearance, broad, with a slight central peak or keel. In cross-section the node apices appear to have a weak dorsal orientation. In dorsal view, the angle between the parietal–squamosal articulations is 164–170°. In dorsal view, the parietal width is the widest part, producing an egg-shaped appearance, but the length and width are more similar, thus producing a more globular than ovoid 'egg'. The overall dorsoventral height of the dome seems shorter than that of ROM 59046, thus producing a lower degree of curvature. In lateral view, the dome is strongly vaulted, with a uniform curvature. The apex of the curvature remains anteriorly on the parietals, but is closer to the frontal–parietal contact. In anterior and posterior views, the curvature towards the apex of the dome gently flattens.

The ventral surface of the frontoparietal dome is in pristine condition. As in *Colepiocephale* (Schott *et al.*, 2009) and *Foraminacephale* (Schott & Evans, 2016), the endocranial fossa is over 50% laterally wider than anteroposteriorly long. In overall morphology, the endocranial fossa is nearly identical to that of *Foraminacephale* (Schott & Evans, 2016). The circular cerebral fossa is approximately 64% the total endocranial fossa anteroposterior length. The anteriormost 60% of the endocranial fossa is on the frontal, and a clear laterally transecting suture between the frontals and parietals is present. The olfactory bulbs, as in *Foraminacephale* (Schott & Evans, 2016), are proportionally small, only acutely diverging and approximately 41% anteroposteriorly longer and laterally wider than the anteroposteriorly short olfactory peduncles. This is unlike that of *Stegoceras* or *Colepiocephale* (Schott *et al.*, 2009), where the olfactory bulbs anterolaterally emarginate and are more equivalent to the cerebral fossa in size.

DMNH EPV.97077

This is the most complete specimen of *Sphaerotholus* thus far found, and in this analysis the specimen was digitally examined (although the specimen has been observed in person by DCE, DCE, and TRL; Fig. 3). Aside from its stature, the most striking aspect of this specimen is that it preserves all of the peripheral elements; the only specimen in the entire genus *Sphaerotholus* with such elements. Unfortunately, due to taphonomic damage, the morphology of many of the more anterior elements (such as the anterior supraorbital) is obscured. In dorsal view there is a large fracture laterally across the dome. Although not perfectly traversing the contact, it would seem that this fracture generally propagates along what might be the frontal–parietal contact. The dorsal surface of the dome has only a few, small 'pits' across it, but given the taphonomic damage to the specimen, we are not certain if these are foramina. Regardless of the distortion, the surface of the dome is smooth, consistent with a greater maturational state. In dorsal view, the angle of the prefrontal–frontal contact is approximately 150°. Overall, the dome is circular in dorsal profile. In lateral view, while both the frontals and parietals are dorsoventrally 'inflated', the parietals are slightly more so. This results in a dome apex that this clearly situated on the parietals and a slight asymmetry in the arc of the dome. This asymmetric arc is more consistent with morphologies seen in smaller, presumably more immature specimens. If correct, this dome size to arc variation may be indicative of body-size plasticity within this species.

In lateral view, posteriorly along the frontoparietal, the slope quickly transitions to the posterior parietal projection. As seen in some other preceding specimens (such as ROM 53584, USNM PAL 537766, MOR 1605 and TMP 1987.113.0003; see Supporting Information), the posterior parietal projection is anteroposteriorly short, but laterally wider than long. Especially clear in dorsal view is the symmetry of the parietosquamosal nodes (particularly on the right node). The parietosquamosal nodes appear to be nearly equally composed of partial and squamosal constituents. Although prominent, all of the ovoid nodes in this specimen are blunted. In dorsal view, the angle between the frontoparietal–squamosal articulations is ~140–155°. Although much of the morphologies of the peripheral elements are taphonomically obscured, one evident informative feature is the presence of the lateral node row. The known *S. buchholtzae* squamosals possess a single posterior node row (TMP 1987.113.0003, ROM 75853, ROM 53582 and ROM 64809; see Supporting Information), and the lateral aspect likewise indicated a single lateral node row. The isolated left postorbital CMN 56510 (*S. buchholtzae*; Mallon *et al.*, 2015) appears to possess a laterally tapered, ~mid-ridge, which would seem to indicate some portion of the lateral node row. DMNH EPV.97077 demonstrates that the lateral node row does indeed anteriorly progress along all of the peripheral elements. This lateral node row is comprised of nodes that decrease in size anteriorly (both in terms of the size of the nodes and their lateral projection) and has a straight anterior trajectory from the squamosal.

DMNH EPV.97077 is one of the only *S. buchholtzae* specimens that preserves any of the basicranial elements (as does DMNH EVP.97076) and, as articulated, they prevent examination of the ventral aspect of the frontoparietal dome.. Future segmentation

of the cranial elements [as done by L. Witmer and colleagues for *Stegoceras validum* (UALVP 2)] will allow for more detailed examination of the braincase.

Variation in parietosquamosal ornamentation

Several squamosals of *Sphaerotholus buchholtzae* have the species-specific and phylogenetic important shape and nodal ornamentation, allowing variation in parietosquamosal bar morphology to be documented for the first time in this taxon (Fig. 4). In addition to the holotype, two specimens (DMNH EPV.97077, ROM 75853) have squamosals articulated with a dome and, therefore, preserve a complete parietosquamosal bar. In these specimens, the squamosals project ventrolaterally (in posterior view), and the node rows are oriented ~24–30° (DMNH EPV.97077; ROM 75853) to ~38° (TMP 1987.113.0003) from the horizontal. In pachycephalosaurs, the orientation of the squamosals (and node rows) can be important phylogenetic and diagnostic characters, as noted by Williamson & Carr (2002). In *S. goodwini*, the squamosals project more ventrolaterally (~47°) than in *S. buchholtzae* (*sensu* Williamson & Carr, 2002). Alternatively, in comparison to *Stegoceras*-grade taxa, such as *Stegoceras validum* and *Prenocephale prenes* Maryńska & Osmólska, 1974, the squamosals are oriented much closer to the horizontal (~16° and ~18°, respectively).

In all *S. buchholtzae* specimens examined here, with one exception (ROM 75835), the squamosal tapers in depth from its maximum thickness at its contact with the parietal to its lateral margin. However, in ROM 75835, the dorsoventral depth of the squamosal is proportionally deeper throughout its length, and it tapers comparatively less. While the orientation of the squamosals does vary between *S. buchholtzae* and *S. goodwini*, both laterally taper (to varying degrees), whereas in *Stegoceras*-grade taxa (*Stegoceras validum* and *Prenocephale prenes*) the squamosals remain uniform in thickness medially to laterally.

The morphology and number of primary parietosquamosal nodes are variable in the sample. For TMP 1987.113.0003, the smallest specimen with articulated squamosals, as well as ROM 64809 (an isolated squamosal), the nodes are triangular in posterior view, and in lateral view, they project dorsally. The posterior surface of each node is slightly

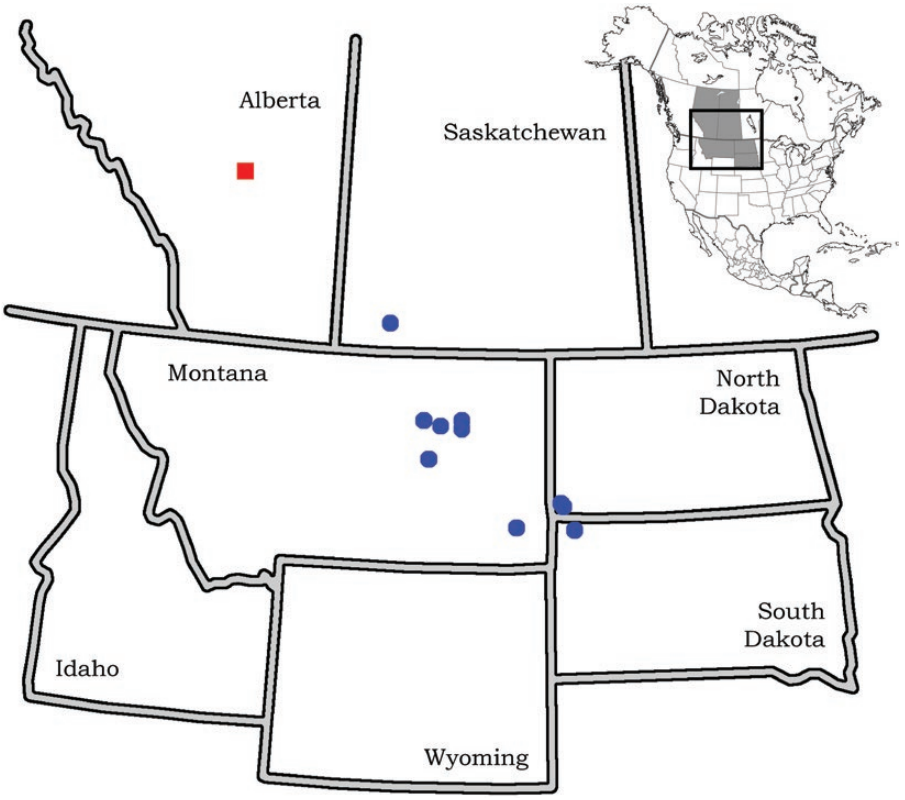

Figure 5. Geographic map showing the distribution of *Sphaerotholus buchholtzae* and *S. edmontonensis* within the United States of America and Canada. Red square = *S. edmontonensis*; blue circle = *S. buchholtzae*.

convex externally, while the anterior surfaces are flat and shallowly inclined. In the largest specimens (ROM 53582 and ROM 75853), all of the nodes are rounded and blunt apically, as has been observed in the size series of squamosals of *Stegoceras validum* (Schott & Evans, 2014) and *Pachycephalosaurus* (Horner & Goodwin, 2009). Previously, the number of nodes reported in the primary node row was four, which was based on the holotype (TMP 1987.113.0003). Several of the new specimens have five nodes in the primary node row, including ROM 64809 and ROM 75853. The number of nodes in the primary node row varies to a similar degree in *Stegoceras validum* and *Prenocephale prenes* (Schott & Evans, 2012; Evans *et al.*, 2018). The position of the medialmost node on either of the midlines varies from being divided by the parietal–squamosal suture in the holotype, to having the medialmost node almost entirely on the parietal in ROM 75835, to almost entirely on the squamosal in ROM 53582. The lateralmost node in the series (the vertex node of Schott and Evans 2012) has a long axis and is typically oriented at a divergent angle (approximately 45°) to the axis of the primary node rows. The relative size of the nodes forming the primary node row are much more variable in ROM 64809 and ROM 75853 than in the holotype and ROM 53582, although this is consistent with the range of variation seen in *Stegoceras validum* (Schott & Evans, 2012). The holotype has an atypical corner node morphology for the sample, where this node is particularly small. In all of the other specimens, the lateroventral corner node is considerably larger, being subequal in size to some of the nodes in the primary node row (ROM 64809, ROM 75853 and ROM 53582). However, in all specimens, the corner node occurs adjacent to the ventral margin of the squamosal, as in *S. goodwini*, but unlike in *Foraminacephale brevis* and *Prenocephale prenes*, where the corner now occurs well above the ventral margin of the squamosal.

Small accessory nodes below the primary node row are present in all of the available specimens. While some shape and size variations are present, all of the specimens possess the smaller accessory node ventral to nodes 3 and 4 (some, such ROM 53582 and ROM 64809, even have an addition node ventral to nodes 2 and 3). Here deemed the posterior accessory node, its presence in every specimen suggests that it may be an autapomorphy for *S. buchholtzae*. A posterior accessory node may be in the holotype of *S. goodwini*. Unfortunately, the right parietal is damaged in this region, so the presence or absence of this node cannot be stated with confidence, and there are no known squamosals for *S. edmontonensis*.

The presence of the tesserate dome surface texture in the anterodorsal region of the squamosal potentially indicates that TMP 1987.113.0003 and ROM 64809 were more immature than either ROM 53582 or ROM 75853. If this is correct, then 'sharp', prominent squamosal nodes may characterize more immature individuals, with nodes rounding with increased age. This has been noted in *Pachycephalosaurus*, but also in *Stegoceras validum* (Schott & Evans, 2012) and *Prenocephale prenes* (Evans *et al.*, 2018).

Histology and relative vascularity

For this analysis, three *S. buchholtzae* specimens spanning the size series and presumed ontogenetic range were CT-scanned and the major histological features and relative void space, a proxy for vascularity, are described here (Fig. 6). The smallest specimen, UCMP 186026, had the largest amount of void space, which was calculated using the Huang thresholding technique at 21.3%. Conversely, the largest specimen scanned, DMNH EPV.97077, had the least amount of void space is 2.5%. The intermediately sized specimen, UWBM 98701, had an intermediate value, at 11.4%. Decreasing void space, a proxy for relative vascularity, through ontogeny is a known ontogenetic feature in other pachycephalosaurs, such as *Stegoceras validum* (20→17→7%; Schott *et al.*, 2011), *Foraminacephale* (1.67→0.84→0.25%; Schott & Evans, 2016) and *Pachycephalosaurus* (Horner & Goodwin, 2009).

The distribution of void spaces throughout the *S. buchholtzae* ontogenetic series also shows a pattern similar to other pachycephalosaurs. In the ontogenetically youngest endmember in the sample set, UCMP 186026, the greatest concentration of void spaces in the frontoparietal are situated ventrolaterally in Zone II (Goodwin & Horner, 2004). In the intermediate ontogenetic stage, UWBM 98701, the void spaces are more radially oriented, proportionally larger and more elongate, and are situated more laterally in the ~lower half of Zone II (Goodwin & Horner, 2004). Finally, in the ontogenetically oldest endmember in the sample set (DMNH EPV.97077), the few remaining void spaces are distributed in the middle of Zone II, deep within the dome (Goodwin & Horner, 2004)

Linear bivariate morphometrics

Linear bivariate regressions based on numerous measurement indices were completed using the *Sphaerotholus* dataset (Fig. 7). Several studies have demonstrated that different pachycephalosaurian genera plot in distinct morphospaces,even based on a few proportional comparisons (Schott *et al.*, 2011; Evans *et al.*, 2013; Schott & Evans, 2016). Here, logarithmic plots were constructed comparing frontoparietal width and thickness, and postorbital length to frontoparietal. The correlation coefficients

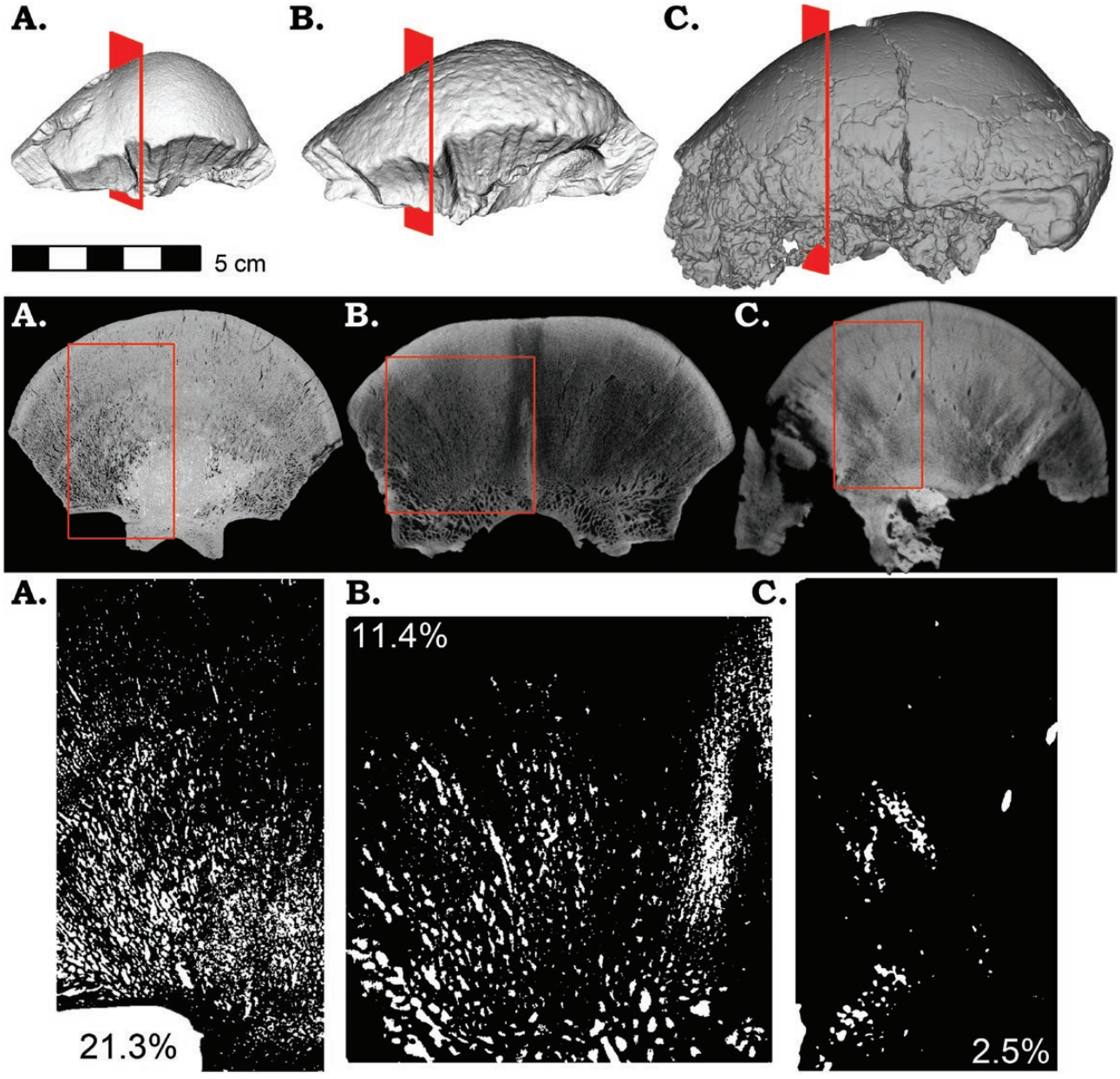

Figure 6. Relative void space (= dome vascularity) decreasing throughout the ontogenetic series of *Sphaerotholus buchholtzae*. A, UCMP 186026; B, UWBM 89701; C, DMNH EPV.97077. All specimens to scale.

for the *S. buchholtzae* specimens were generally high (0.9) and, as Schott & Evans (2016) have demonstrated for *Foraminacephale brevis*, high correlation values support the specimens representing an ontogenetic series (e.g. Dodson, 1975). Frontoparietal length and thickness exhibited positive allometry (r^2 above 0.92) and weakest allometry when compared to width. The greatest slope was represented by frontoparietal length vs. width (*S. buchholtzae* 1.42; *Foraminacephale* 1.21) and the lowest frontoparietal thickness vs. width (*S. buchholtzae* 1.11; *Foraminacephale* 0.74).

In addition to the *S. buchholtzae* specimens, *S. edmontonensis*, *S. goodwini*, *Foraminacephale brevis* and *Prenocephale prenes*. *Foraminacephale brevis* and *P. prenes* were included because these taxa had previously been referred to, or associated with, *Sphaerotholus*. Unfortunately, *S. edmontonensis*, *S. goodwini* and *P. prenes* were only represented by a single specimen herein (CMN 8830, NMMNH P-27403, Z. Pal. No. MgD-I/104, respectively), so we were unable to compare ontogenetic trajectories of size in these taxa. In this comparative analysis, where

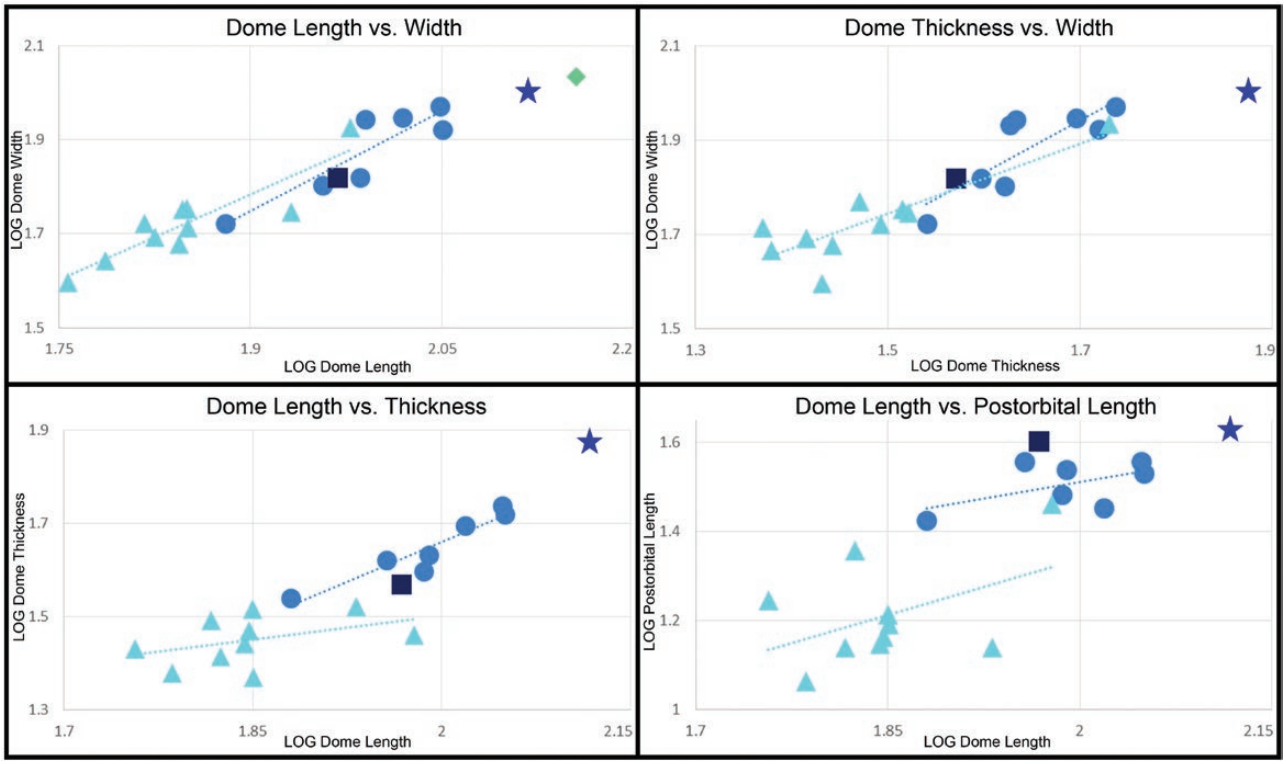

Figure 7. Linear bivariate logarithmic plot of examined pachycephalosaurids. All square = *Sphaerotholus edmontonenesis*; stars = *S. goodwini*; circles = *S. buchholtzae*; triangles = *Foraminacephale brevis*; diamond = *Prenocephale prenes*. L:W = length to width of the frontoparietal dome; T:W = thickness to width of the frontoparietal dome; L:T = length to thickness of the frontoparietal dome.

the specimens recorded the appropriate data, both *S. goodwini* (NMMNH P-27403) and *P. prenes* (Z. Pal. No. MgD-I/104) are distinct from the *S. buchholtzae* trajectory. Interestingly, *S. edmontonensis* (CMN 8830) clustered tightly with that of *S. buchholtzae* in all bivariate comparisons in this study. Within the *S. buchholtzae* trajectories, *S. edmontonensis* (CMN 8830) consistently plotted with smaller and presumably younger specimens. *Foraminacephale brevis* plots closely to *S. buchholtzae* in most comparisons.

Two-dimensional geometric morphometrics (2D GM)

Landmark-based geometric morphometric analysis with both immature and mature frontoparietal domes of *S. buchholtzae* were used to describe possible ontogenetic morphological changes and to compare *S. buchholtzae* to other taxa at as many developmental stages as possible. Lateral and dorsal views of complete frontoparietals were each analysed to capture overall morphology. These orientations were also used in earlier pachycephalosaurid analyses by Chapman *et al.* (1981) and Goodwin (1990). In both lateral and dorsal views, the first four PC axes describe over 80% of the variation. Initially, one may predict morphospace patterns similar to the linear results. Interestingly, for the lateral 2D GM, each species of *Sphaerotholus* plotted in its own distinct and unique morphospace along the first two major axes of variation (Fig. 8). In the lateral view analysis, PC 1 accounts for 40.3% of the variability and PC 2 for 21.5% (PC 3 11.4%, PC 4 8.7%, PC 5 6.3%, PC 6 4.6%; Table 2). In lateral orientation, most landmarks correspond to sutural contact locations. The eigenvectors reveal that the location of landmarks associated with nasal, prefrontal, postorbital, squamosal margins and the dome apex were all important. The most significant landmark was the position of the contacts between the posterior supraorbitals and the postorbitals. While the lateral profiles of the three *Sphaerotholus* species appear similar (particularly *S. buchholtzae* and *S. edmontonensis*), the 2D GM revealed distinct morphology of each taxon.

As in the lateral 2D GM, the dorsal 2D GM likewise show that the three *Sphaerotholus* species occupy unique morphospaces (Fig. 9): PC 1 accounts for 56.8% of the variability, PC 2 for 18.2% and PC 3 13.3% (Table 3). However, unlike the two-dimensional lateral analysis, the three species of *Sphaerotholus*

Table 2. Lateral 2D PCA scores

	PC 1	PC 2
x1	–0.02434276	0.2000175986
y1	–0.23032891	–0.23032891
x2	–0.02359633	0.0004014191
y2	–0.12532187	0.0499313030
x3	–0.07996316	0.1492610608
y3	–0.11676418	–0.0706284575
x4	–0.27389201	0.0154507590
y4	0.05140772	0.1009238327
x5	–0.13155520	0.0157447850
y5	0.01479925	–0.0821426646
x6	–0.10693425	–0.1210884246
y6	0.06204115	0.1278523733
x7	0.06951352	–0.1234521381
y7	0.07449982	–0.0994644216
x8	–0.03333721	–0.2221333544
y8	0.13051687	0.1384760468
x9	0.52573669	–0.3311643633
y9	0.28696290	–0.0553348913
x10	0.39154771	–0.2306909761
y10	0.13451429	0.1504408186
x11	0.16377051	0.5069354650
y11	0.04338269	–0.0666431639
x12	0.15858446	0.4416781848
y12	–0.05924673	0.1116977874
x13	0.05256092	–0.0224795475
y13	–0.03171819	–0.0970521595
x14	–0.1357777034	–0.1357777034
y14	–0.05440986	0.1281627828
x15	–0.23626092	0.0051567589
y15	–0.07163640	–0.0157711252
x16	–0.19442149	–0.1478595239
y16	–0.10869856	–0.2387137143

do not overlap only on the first axis of variation. An association of higher eigenvalues in regions of the dome related to lateral expansion by the anterior and posterior supraorbitals and the postorbitals was confirmed in dorsal orientation. As in the lateral analysis, significant loci are those associated with lateral expansion of the dome through ontogeny.

Sphaerotholus edmontonensis (CMN 8830) plotted in a relatively similar space as observed in the lateral 2D GM, but *S. goodwini* (NMMNH P-27403) plotted in a nearly opposing location in dorsal view (positive PC 2 axis lateral; negative PC 2 axis dorsal). The only observed morphospace overlap was between *S. buchholtzae* and *Foraminacephale* in PC 2; one of the smaller and presumably more immature *Foraminacephale* specimens (ROM 53603) overlaps the morphospace on this axis with the smaller and more immature *S. buchholtzae* specimens.

Three-dimensional geometric morphometrics (3D GM)

The 3D GM analysis reveals more dramatic segregation of morphospaces by taxon than observed in either of the 2D analyses (Fig. 10). The first three PC axes account for over 97% of the variability: PC 1 and PC 2 account for the greatest variation (69.5% and 18.5%, respectively, with PC 3 comprising 10.3% (Table 4). Eigenvectors of individual landmarks show that the most variation occurs in similar regions identified by 2D analyses, notably the posterior supraorbital and the postorbital sutural contacts. In 3D PC 1 scores (Table 4), the most significant region pertains to the posterior parietal process, especially those related to the dorsoventral height of and posterior length of this process.

Overall, the 3D PCA shows segregations of the three *Sphaerotholus* species. The three *Sphaerotholus* species do not overlap in PC 1 or 2. In PC 1 and 2, the single specimens of *S. edmontonensis* and *S. goodwini* are on the negative end of this axis, with both being widely separated from *S. buchholtzae.* In PC 1, there is a minor degree of morphospace overlap between *S. buchholtzae* and *Foraminacephale*, but separate clusters for these genera can be discerned. It is noteworthy that in the first three 3D PC axes, the *S. buchholtzae* and *Foraminacephale* occupy similar morphospaces and are morphologically more similar to each other than either is to *S. edmontonensis* and *S. goodwini*. The clusters of the former taxa encompass the range of observed size and ontogenetic variation in these species. Even given the paucity of *S. edmontonensis* and *S. goodwini* data points, we may have predicted less disparity between taxa – as observed in the linear bivariate logarithms.

While the 2D and 3D analyses emphasize distinct regions of significance, they all indicate that morphologies of the peripheral elements, particularly the elements flanking the frontoparietal contact, are morphometrically significant in differentiating *Sphaerotholus* species.

While the ontogenetic changes observed within *S. buchholtzae* are not as dramatic as that of hadrosaurs or ceratopsians, at least in part because only a fraction of the ontogenetic stages are currently known from fossils, we document distinct ontogenetic changes between the ontogenetically youngest and oldest specimens [or ontogimorphs *sensu* Goodwin & Evans (2016); Fig. 11]. Given the limited sample sizes, the 3D GM analysis was able to closely associate species

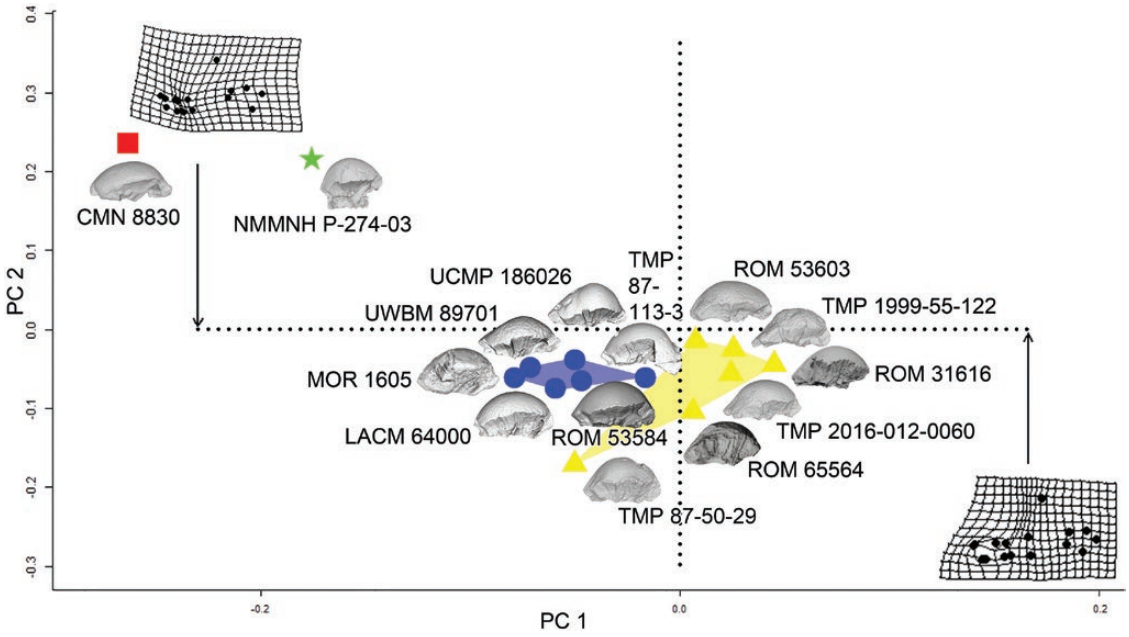

Figure 8. Two-dimensional geometric morphometric principal component analysis of examined pachycephalosaurines in lateral view. Red square = *Sphaerotholus edmontonenesis*; green star = *S. goodwini*; blue circle = *S. buchholtzae*; yellow triangle = *Foraminacephale brevis*. Blue polygonal space is the enveloping morphospace occupied by *S. buchholtzae*. Large yellow triangular space is the enveloping morphospace occupied by *Foraminacephale brevis*. Specimens not to scale.

regardless of this ontogenetic variability, indicating that the overall dome morphology of these species changes relatively little over their known ranges.

A comparison of the 3D PCA scores to LOG frontoparietal lengths indicates that the frontoparietal changes shape with increasing size in both PC1 and PC2 (Fig. 12; Table 5). While both PC1 and PC2 have similar trends relative to frontoparietal length, their ontogenetic distributions slightly vary. For both PC1 and PC2, LACM 64000 appears more of an 'outlier' by not closely following the observed ontogenetic pattern. This is most noticeable in the PC1 regression, where LACM 64000 is distinct on the PC axis from the other specimens, most likely individual variation within the species. As noted earlier in the above description, LACM 64000 is symmetrically domed in lateral profile, while in dorsal view the dome has a reduced ovoid profile in contrast to the egg-shaped, posteriorly wider expression in more mature specimens. The odd placement of LACM 64000 here could reflect its 'non-typical' frontoparietal morphology in the same way 3D GM was able to capture the pathologic UWBM 89701.

Stratigraphy

Precise stratigraphic locations are currently only known for some of the *Sphaerotholus* specimens. Seven (DMNH EPV.97077, DMNH EPV.97076, DMNH EPV.97078, TMP 1987.113.0003, UCMP 186026, UWBM 89701 and ROM 75853) are known with precise measurement from a stratigraphic datum (typically the K–Pg Boundary) and the majority of the remaining specimens are known more generally within the context of the tripartite division of the Hell Creek Formation into upper, middle and lower informal units of Horner *et al.* (2011; Fig. 13). The majority of the specimens examined here originate from the lower and middle third of the Hell Creek Formation (Fig. 13). Based on our qualitative stratophenetic assessment of the available material, with particular emphasis on dome shape and parietosquamosal ornamentation, *S. buchholtzae* appears to be fairly uniform in morphology through its biostratigraphic range within the Hell Creek Formation.

Phylogenetic analysis

The parsimony analysis resulted in 89 most0parsimonious trees (MPTs), each with a tree length of 91, a consistency index (CI) of 0.6707, a homoplasy index (HI) of 0.3293, a retention index (RI) of 0.7939 and a rescaled consistency index (RCI) of 0.5583. Both the Bayesian and parsimony analyses produced superficially similar topologies (Fig. 14).

In the strict consensus tree of the parsimony analysis, Pachycephalosauridae consists of a *Stegoceras* clade that is comprised of a large polytomy of *Hanssuesia sternbergi* (Brown & Schlaikjer, 1943),

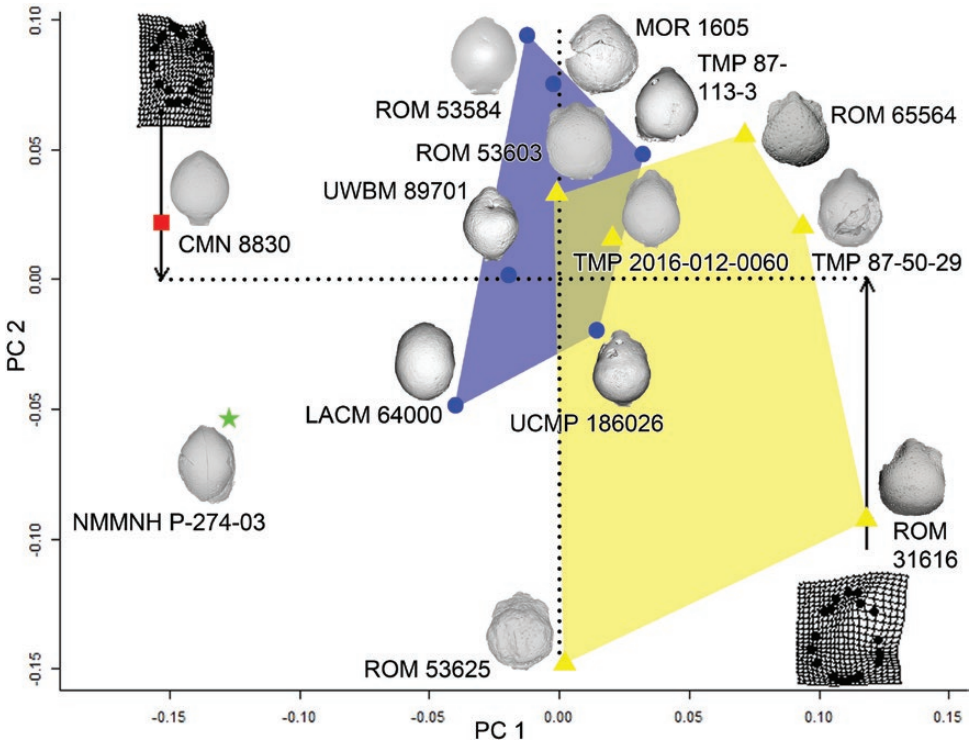

Figure 9. Two-dimensional geometric morphometric principal component analysis of examined pachycephalosaurines in dorsal view. Red square = *Sphaerotholus edmontonenesis*; green star = *S. goodwini*; blue circle = *S. buchholtzae*; yellow triangle = *Foraminacephale brevis*. Blue polygonal space is the enveloping morphospace occupied by *S. buchholtzae*. Large yellow polygonal space is the enveloping morphospace occupied by *Foraminacephale brevis*. Specimens not to scale.

Colepiocephale lambei, *Stegoceras validum*, and *S. novomexicanum* Jasinski & Sullivan, 2011. The sister-taxon of the *Stegoceras* clade is Pachycephalosaurinae, which is largely unresolved. Synapomorphies of Pachycephalosaurinae include the closure of the supratemporal fenestrae (Character 28) and the caudal margin of the parietals blending with the parietosquamosal shelf along the curvature of the dome (Character 34). Within the large Pachycephalosaurinae polytomy, several small clades are recovered. *Goyocephale lattimorei* Perle *et al.*, 1982 and *Homalocephale calathocercos* Maryanska & Osmolska, 1974 are recovered as sister-taxa, and *Dracorex hogswartsia* Bakker *et al.*, 2006, *Stygimoloch spinifer* Galton & Sues, 1983 and *Pachycephalosaurus wyomingensis* are united within the previously recognized Pachycephalosaurini (Sullivan, 2006; Longrich *et al.*, 2010) by the presence of a long rostrum (Character 26) and by large nodes projecting laterally from the jugal (Character 47). Importantly, the three species of *Sphaerotholus* are recovered in an unresolved *Sphaerotholus* clade. This *Sphaerotholus* clade is defined by: the dorsal margins of postorbital and posterior supraorbital sutures dorsally arch with a distinct dividing diastema (Character 33), the parietosquamosal bar is steeply sloped at a ventrolateral angle in caudal view (Character 35), the parietosquamosal bar shallows laterally (Character 36) and the presence of a parietosquamosal node (Character 42). According to the parsimony analysis, of the three *Sphaerotholus* species, *S. goodwini* also has unambiguous autapomorphic characters: a restricted exposure of the intersquamosal process (Character 37) and a partial node on the parietal that corresponds to a counterpart on the squamosal (Character 42).

The Bayesian analysis recovered a largely congruent typology to that of the strict consensus tree in the parsimony analysis. The primary difference in the two analyses is that the Bayesian 50% majority rule summary tree has a slightly more resolved Pachycephalosaurinae, with *Foraminacephale brevis* and *Amtocephale gobiensis* Watabe *et al.*, 2011 occurring as successive sister-taxa to a larger, mostly unresolved group of pachycephalosaurines. Additionally, *Alaskacephale gangloffi* Sullivan, 2006 is alternatively recovered as the sister-taxon to the Lancian Pachycephalosaurini. Finally, as in the parsimony analysis, all three species of *Sphaerotholus* are united into one clade. However, in the Bayesian analysis, *S. edmontonensis* and *S. buchholtzae* are

Table 3. Dorsal 2D PCA scores

	PC 1	PC 2
x1	–0.170480861	–0.023783598
y1	–0.119174414	0.153071064
x2	–0.017190267	–0.066180593
y2	0.061106495	0.137278836
x3	–0.090113216	–0.008386614
y3	–0.206828480	0.212049987
x4	–0.018581910	–0.017263236
y4	0.101337471	0.110011084
x5	0.313741466	0.035670264
y5	–0.319312078	0.150751971
x6	0.128970832	–0.090596694
y6	0.240336707	0.010159982
x7	–0.043181805	0.191936571
y7	–0.115257039	0.001067618
x8	–0.039551112	0.079992269
y8	0.142129357	–0.307980803
x9	–0.024746152	–0.044623424
y9	0.282154445	–0.220517684
x10	–0.003700732	0.184574379
y10	0.158647120	0.007464218
x11	–0.013706968	–0.172956859
y11	0.505498057	0.066998177
x12	0.191188605	0.163344184
y12	–0.173657035	0.010437287
x13	–0.225179982	–0.160762703
y13	–0.142860547	–0.072518825
x14	0.156860899	0.441806547
y14	–0.073134426	–0.174583321
x15	–0.072344511	–0.434132002
y15	0.005121785	–0.244490437
x16	–0.035999135	0.130994209
y16	–0.154139408	0.083742403
x17	0.005973123	–0.188463992
y17	–0.090980526	–0.035210141
x18	–0.041958273	–0.021168707
y18	–0.100987485	0.112268585

sister-taxa, while *S. goodwini* is recovered as sister to the *S. edmontonensis–S. buchholtzae* pair.

In the strict consensus tree based on the parsimony analysis, the three *Sphaerotholus* species form an unresolved clade; yet in the Bayesian analysis, *S. buchholtzae* and *S. edmontonensis* are more closely related to each other within the clade of the three *Sphaerotholus* species. In the parsimony analysis, *Pachycephalosaurus wyomingensis*, *Stygimoloch spinifer* and *Dracorex hogwartsia* form a clade in which the latter two taxa are sister-taxa with *Pachycephalosaurus* as the basalmost member. The Bayesian analysis found the same relationships of these Hell Creek operational taxonomic units (OTUs), and *Alaskacephale gangloffi* is in turn the sister-taxon to this clade, as part of the Pachycephalosaurini lineage. Finally, the parsimony analysis recovered a largely unresolved Pachycephalosaurinae (consisting of *Foraminacephale brevis*, *Amtocephale gobienses*, *Goyocephale lattimorei*, *Homalocephale calathocercos*, *Tylocephale gilmorei* Maryańska & Osmólska, 1974, *Prenocephale prenes*, *Acrotholus audeti* Evans *et al.*, 2013, *Dracorex hogwartsia*, *Stygimoloch spinifer*, *Pachycephalosaurus wyomingensis*, *Alaskacephale gangloffi*, *Sphaerotholus goodwini*, *S. buchholtzae* and *S. edmontonensis*). Conversely, the Bayesian analysis produces greater resolution with *Foraminacephale brevis* recovered as the sister-taxon to all other Pachycephalosaurinae, then *Amtocephale gobiensis*, followed by a clade consisting of the remaining pachycephalosaurines.

SYSTEMATIC PALAEONTOLOGY

DINOSAURIA OWEN, 1842

ORNITHISCHIA SEELEY, 1888

PACHYCEPHALOSAURIA MARYANSKA & OSMÓLSKA, 1974

PACHYCEPHALOSAURIDAE STERNBERG, 1945

PACHYCEPHALOSAURINAE SERENO, 1997

SPHAEROTHOLUS WILLIAMSON & CARR, 2002

Type species: Sphaerotholus goodwini Williamson & Carr, 2002.

Diagnosis (following Williamson & Carr, 2002): Differs from all other pachycephalosaurids in the possession of the following unique combination of characters: a parietosquamosal bar that decreases in depth laterally as seen in caudal view and is bordered by a single primary row of four to five nodes plus one lateroventral corner node located directly below the lateralmost node in the primary node row. This genus currently includes three known species: *S. buchholtzae*, *S. edmontonensis* and *S. goodwini*.

SPHAEROTHOLUS BUCHHOLTZAE WILLIAMSON & CARR, 2002

Stegoceras edmontonense (Brown & Schlaikjer, 1943). Giffin, 1989: 528, fig. 5.

Prenocephale edmontonensis (Brown & Schlaikjer, 1943). Sullivan, 2000a: 178, figs 1, 2.

Prenocephale edmontonensis (Brown & Schlaikjer, 1943). Sullivan 2006: 353, fig. 4.

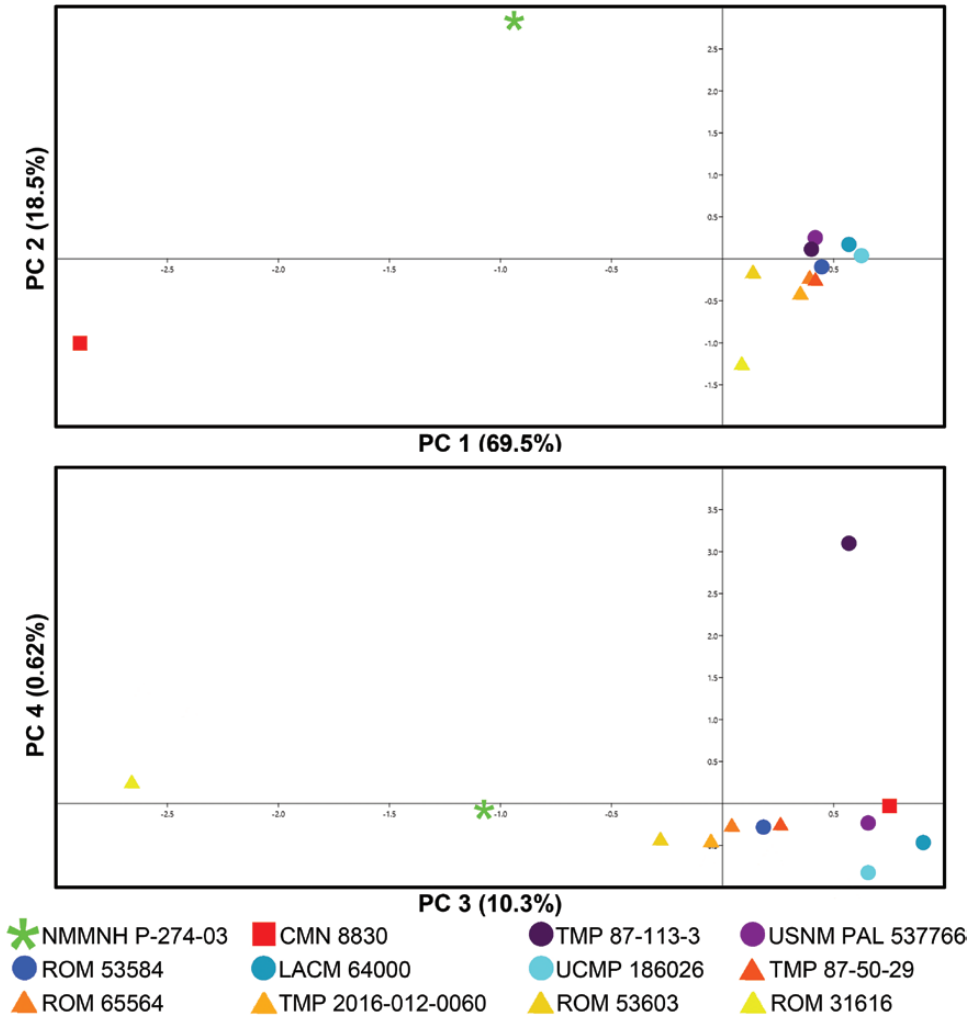

Figure 10. Three-dimensional geometric morphometric principal component analysis of examined pachycephalosaurines. Red square = *Sphaerotholus edmontonenesis*; green star = *S. goodwini*; blue circles = *S. buchholtzae*; yellow triangles = *Foraminacephale brevis*. Specimens not to scale.

Holotype: TMP 1987.113.0003.

Locality and horizon: SE1/4, Sec. 5, T1S, R55E; Carter County, Montana; Upper portion of the Hell Creek Formation.

Diagnosis (following Williamson & Carr, 2002): Differs from all other pachycephalosaurids in the following unique combination of characters: a parietosquamosal bar that strongly decreases in depth laterally as seen in caudal view, the primary node row consists of four nodes with one small lateroventral corner node, wide intersquamosal process of the parietal that captures a medial portion of the medialmost primary node. Differs from *S. edmontonensis* (see below) in the relative length of the postorbital and parietal region of skull at similar frontoparietal size.

Referred material: UCMP 186026, smallest specimen in the dataset, complete frontoparietal dome of immature individual; UWBM 89701, complete 'intermediate sized' frontoparietal dome of immature individual; ROM 53584, complete frontoparietal dome of a large individual; DMNH EPV.97077, complete frontoparietal dome, one of the largest specimens in the dataset (Fig. 3). For a complete list of specimens referred to the hypodigm and their provenances see Table 1 and cranial morphological descriptions in the Supporting Information.

Locality and horizon of referred material: All of the material was collected from the Hell Creek Formation of Montana, North Dakota and South Dakota, with one specimen from the Frenchmen Formation of Saskatchewan (Mallon *et al.* 2015; Fig. 5). Specimens

Table 4. 3D PCA scores

	PC 1	PC 2
x1	0.06397214	–0.073038563
y1	0.005411875	0.160298824
z1	–0.111230943	–0.092097683
x2	0.133281643	–0.005649822
y2	0.02872915	0.14731791
z2	–0.045236843	–0.113339687
x3	–0.028584948	0.144728846
y3	–0.11485368	0.052915544
z3	–0.088872984	–0.047437706
x4	0.053303753	0.129284538
y4	0.140715786	–0.026018042
z4	–0.00069472	–0.140977547
x5	0.124669004	–0.003021304
y5	–0.063338399	0.106303483
z5	–0.12422343	–0.073766749
x6	0.071895218	–0.105488388
y6	–0.141642449	–0.023653684
z6	–0.076839529	–0.149936221
x7	–0.126814786	0.076890054
y7	0.12222937	0.05721512
z7	–0.120003303	–0.084801008
x8	–0.101220297	0.101609229
y8	0.153841706	–0.010698006
z8	–0.065377217	–0.132120696
x9	0.088842501	–0.129083795
y9	–0.042034455	0.12154499
z9	0.089384038	–0.078994521
x10	0.122650016	–0.087006883
y10	–0.008718699	0.171843687
z10	0.100520234	–0.061163872
x11	–0.131425591	0.071417367
y11	0.13179559	0.041167327
z11	–0.136518305	–0.066761081
x12	–0.046004028	0.158472064
y12	0.133949961	–0.050657589
z12	–0.128545556	–0.037965382
x13	0.152499701	–0.038384631
y13	–0.095559138	0.126251799
z13	0.039897919	–0.131765851
x14	–0.031810084	–0.154367521
y14	–0.145338044	–0.073570633
z14	0.144225401	0.014928327
x15	–0.087696166	0.121524778
y15	–0.028121536	–0.037204886
z15	0.00759682	0.04831551
x16	–0.087230308	0.149645502
y16	0.099254577	–0.140999711
z16	0.05925552	–0.062838082
x17	–0.073888166	–0.013703207
y17	0.032621933	0.158175148
z17	0.053487772	–0.085414835

Table 4. Continued

	PC 1	PC 2
x18	–0.094071022	–0.140442877
y18	–0.138190427	–0.076532326
z18	0.148913361	0.057926324
x19	0.134407659	–0.060538856
y19	0.060306628	–0.126346959
z19	–0.027237954	0.144296726
x20	0.151223692	–0.058018544
y20	0.066195266	–0.132351277
z20	–0.07726892	0.122543093
x21	–0.110856008	–0.132420738
y21	–0.121347892	–0.096436353
z21	0.110163803	0.106929246
x22	–0.107717316	–0.135306783
y22	–0.130626325	–0.086441326
z22	0.083724202	0.109119963
x23	0.14209667	0.087500895
y23	0.070967431	–0.130052339
z23	0.008900414	0.116024024
x24	0.140976422	0.074939475
y24	0.105461556	–0.126489167
z24	–0.05848137	0.042477938
x25	0.138498453	0.078225873
y25	0.014102395	0.042915814
z25	0.051508101	–0.00823717
x26	0.136307212	0.078562498
y26	–0.046057593	0.082197168
z26	0.101110211	–0.037836049
x27	0.130667689	0.059506358
y27	0.003322143	–0.067451128
z27	0.017366024	0.139607593
x28	0.118916634	–0.03263507
y28	0.121484253	0.064803763
z28	–0.026458579	–0.06686715
x29	0.150155666	0.068902543
y29	0.071360219	–0.081978254
z29	0.0691826	0.002533602
x30	0.135762375	–0.065370364
y30	0.048389704	0.154557052
z30	0.011096187	–0.136667016
x31	0.061003855	0.042938662
y31	–0.012101984	0.172351675
z31	0.043895907	–0.11557172
x32	0.146044285	0.03746988
y32	0.033898432	0.101749492
z32	0.009620329	–0.040324615
x33	0.0748988	–0.023515983
y33	0.010195311	0.078979828
z33	0.012937429	–0.054853104
x34	–0.122815895	0.047652974
y34	–0.122834711	0.012678747
z34	–0.038681475	0.107832354

Table 4. Continued

	PC 1	PC 2
x35	–0.087040226	0.123187802
y35	0.126818529	0.061261926
z35	–0.127156108	0.034983404
x36	–0.063437968	0.069614489
y36	0.022214922	0.126577938
z36	–0.127201821	0.056819073

occur throughout the Hell Creek Formation and the taxon has an age range of ~67.20–66.05 ± 0.008 Mya (Williamson & Carr, 2002; Mallon *et al.*, 2015; Fowler, 2017; Sprain *et al*., 2018). See Table 1 for provenance of all specimens assigned to this taxon.

Comments: Frontoparietals that lacks an associated squamosal were assigned to *S. buchholtzae* based on a wide intersquamosal process with nodes shared between parietal and squamosal. *Sphaerotholus edmontonensis* was considered distinct from *S. buchholtzae* based on the results outlined below and the conclusions by Mallon *et al.* (2015) (*contra* Sullivan, 2006). The assignment of poorly preserved paratype material of *S. edmontonensis* from the Horseshoe Canyon Formation was based on formational provenance and co-occurring morphology to the type (see below). Even though DMNH EPV.97077 is from the Hell Creek Formation of south-western North Dakota, Bourke *et al.* (2014) identify it as *Sphaerotholus edmontonensis* following, in part, Sullivan (2000) in which the species *S. buchholtzae* is considered a subjective junior synonym of *S. edmontonensis*. We disagree with this referral. Our results support *S. edmontonensis* and *S. buchholtzae* as distinct taxa following Longrich *et al.* (2010) and Mallon *et al.* (2015). DMNH EPV.97077 is diagnostic and recognized here as *S. buchholtzae*. In DMNH EPV.97077, there is only a single node row, the parietosquamosal bar tapers laterally, the squamosal bears a prominent corner node and the posterior parietal process is wide but relatively short. The identification of DMNH EPV.97077 [and two other specimens found in close proximity, DMNH EPV.97076 and DMNH EPV.97078; and formerly catalogued as Marmarth Research Foundation specimens (Bourke *et al.*, 2014)] as *S. buchholtzae* is also consistent with the stratigraphic occurrence of *S. buchholtzae* in the latest Maastrichtian (Mallon *et al.*, 2015).

SPHAEROTHOLUS EDMONTONENSIS (BROWN & SCHLAIKJER, 1943)

Holotype: CMN 8830, a complete but weathered frontoparietal dome.

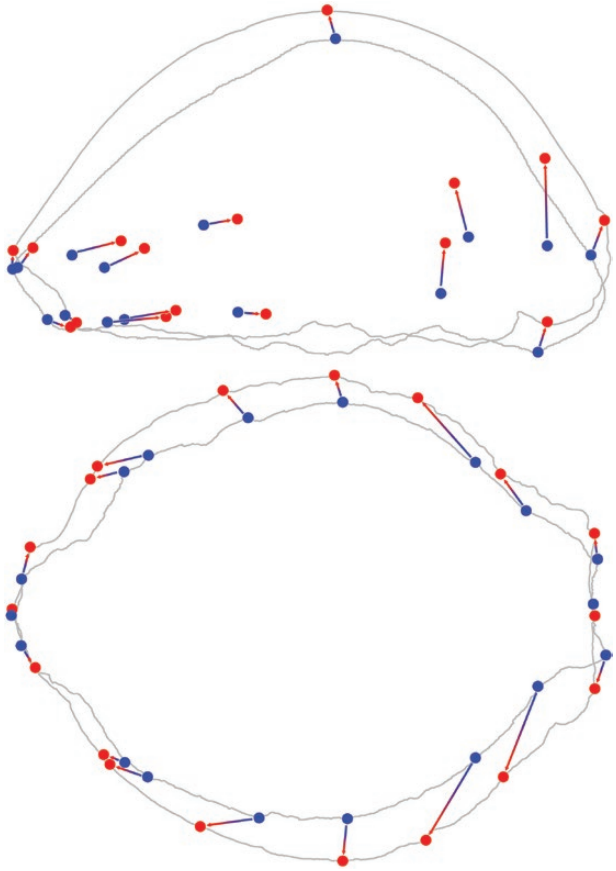

Figure 11. Ontogenetic development of landmark positions in *Sphaerotholus buchholtzae* in dorsal (top) and left lateral (bottom) orientations. Blue landmarks are the immature UCMP 186026, while red landmarks are from the mature ROM 53584. Grading arrows denote the transition of landmarks.

Locality and horizon: Tolman Member of the Horseshoe Canyon Formation, Alberta (Eberth *et al.*, 2013). Age: ~68.4 – 70.9 Mya; Eberth *et al.*, 2013; Fowler, 2017.

Referred material: CMN 8831 (paratype) incomplete frontoparietal dome; CMN 8832, (paratype) incomplete frontoparietal dome.

Comments: All of the known material of this taxon is derived from the Tolman Member of the Horseshoe Canyon Formation, Alberta (Eberth *et al.*, 2013) and is, therefore, earliest Maastrichtian in age.

Previous diagnosis: 'Differs from *S. goodwini* in that the parietals are broad posteriorly and bear a pair of nodes, and *S. edmontonense* can be distinguished from *S. buchholtzi* [*sic*; *S. buchholtzae*] by the longer parietals" (Longrich *et al.*, 2010).

Revised diagnosis: Small pachycephalosaurine pachycephalosaurid united within the *Sphaerotholus* clade by: dorsal margins of postorbital and posterior supraorbital sutures dorsally arched with distinct dividing diastema (Character 33), parietosquamosal bar steeply sloped at ventrolateral angle in caudal view (Character 35), parietosquamosal bar shallows laterally (Character 36), possesses a parietosquamosal node (Character 42). Distinguishing characteristics include: anteroposterior length of the postorbital and anterior supraorbital are relatively longer than that of *S. buchholtzae*, peripheral element sutural contacts that proportionally vary compared to equivalent sized *S. buchholtzae* (height of the nasal contact, height of the prefrontal and anterior supraorbital contact, thickness of the frontoparietal, length of the posterior supraorbital, length of the postorbital, width between the nasal and prefrontal contact, and width between the posterior contacts of the parietal), a convex peripheral element profile (prefrontal–squamosal), and a rectangular posterior parietal process compared to equivalently sized *S. buchholtzae*.

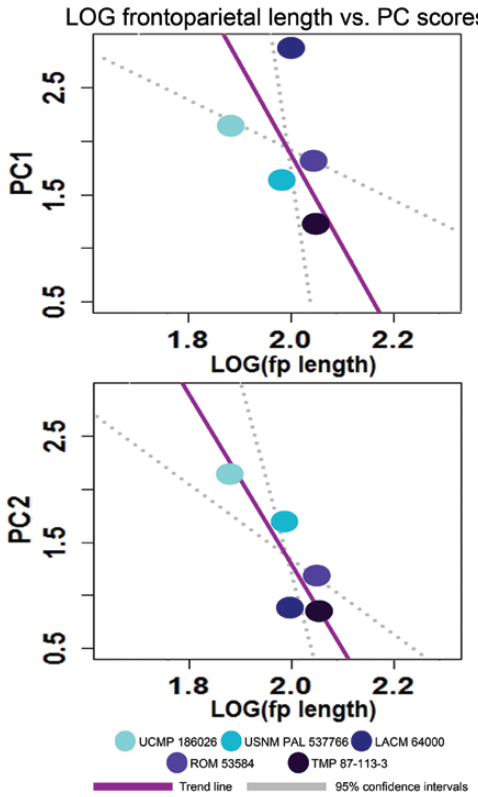

Figure 12. LOG frontoparietal length versus 3D PCA in *Sphaerotholus buchholtzae*.

Nomenclatural comment: A notable peculiarity to the history of *S. edmontonensis* is the spelling variants of its epithet. In the first description of CMN 8830 (originally GSC 8830), Brown & Schlaikjer (1943) originally refer to the specimen as '*Troödon*' *edmontonensis*, and this spelling was used in subsequent works in the 1940s (such as in Sternberg, 1945). In 1987, the spelling changed in Sues and Galton's review of North American pachycephalosaurs. In their review, Sues & Galton (1987) note that the etymology of *edmontonensis* is the neo-Latin derivative from its occurrence in the former Edmonton Formation. Yet, proceeding this passage, Sues & Galton (1987) adopt the spelling as *edmontonense*. While in neo-Latin, location is by default masculine (i.e. -sis), the suffix –se can be used in Contemporary Latin to denote femininity. Immediately preceding their discussion on *edmontonense*, Sues & Galton (1987) state that, '… Chapman *et al.* (1981) clearly demonstrated that the supposed specific differences are, in fact, size dependent and subject to sexual dimorphism.… The phenon with the larger, thicker, and more convex domes was identified by Chapman *et al*. as "male" and the phenon with the smaller, less convex domes as "female".' Throughout the rest of the paper, Sues & Galton (1987) ascribe to the 'low dome = female; high dome = male' hypothesis of Chapman *et al.* (1981). Although they do not specifically address the sex of CMN 8830, we surmise that, given the small stature and low dome profile of CMN 8830, Sues & Galton (1987) thought the specimen was female (in this case the 'female from the Edmonton Formation') and, consequently, altered the spelling to reflect such.

Given that at the time of Sues & Galton (1987), the discipline did not know of the complex ontogenetic changes associated with pachycephalosaurid dome development (Horner & Goodwin, 2009; Evans *et al.*, 2011; Schott *et al.*, 2011; Goodwin & Evans, 2016; Schott & Evans, 2016), such a referral was

Table 5. *Sphaerotholus buchholtzae* frontoparietal length vs. PC scores

Frontoparietal length vs.PCA scores	N	Slope (m)	95% CI (m)	Intercept (b)	95% CI (b)	R2	Trend
PC1	5	–8.726212	6.623172 66.54480	–8.726212	–32.416649 –2.349002	0.120825	neg
PC2	5	17.25340	8.3508986 37.48706	–7.976780	–18.12969 –3.5096591	0.7512402	neg

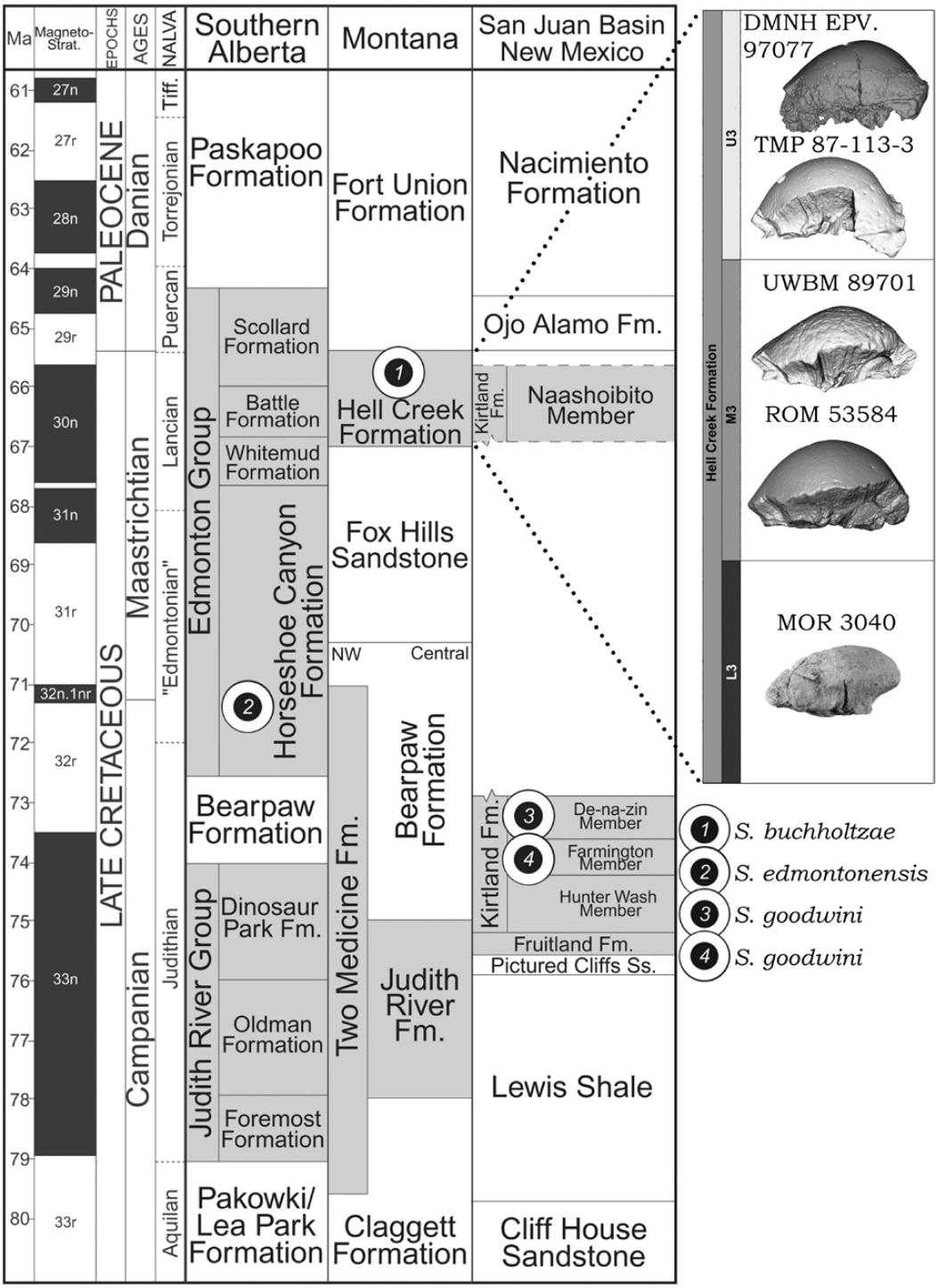

Figure 13. A, stratigraphic distribution of the three *Sphaerotholus* species throughout the Late Cretaceous. 1, *S. buchholtzae*; 2, *S. edmontonensis*, 3, *S. goodwini*. Stratigraphic section modified from Williamson & Carr (2002). B, distribution of *S. buchholtzae* specimens throughout the Hell Creek Formation. Modified from Williamson & Carr (2002). Specimens not to scale.

based on supporting information at the time (like other feminizing suffixes, i.e. *Maiasaura*). However, this change has caused a ripple in subsequent pachycephalosaurid works. In post-Sues & Galton (1987) studies, *S. edmontonense* is used by Giffin (1989), Williamson & Carr (2002), Maryańska *et al.* (2004),

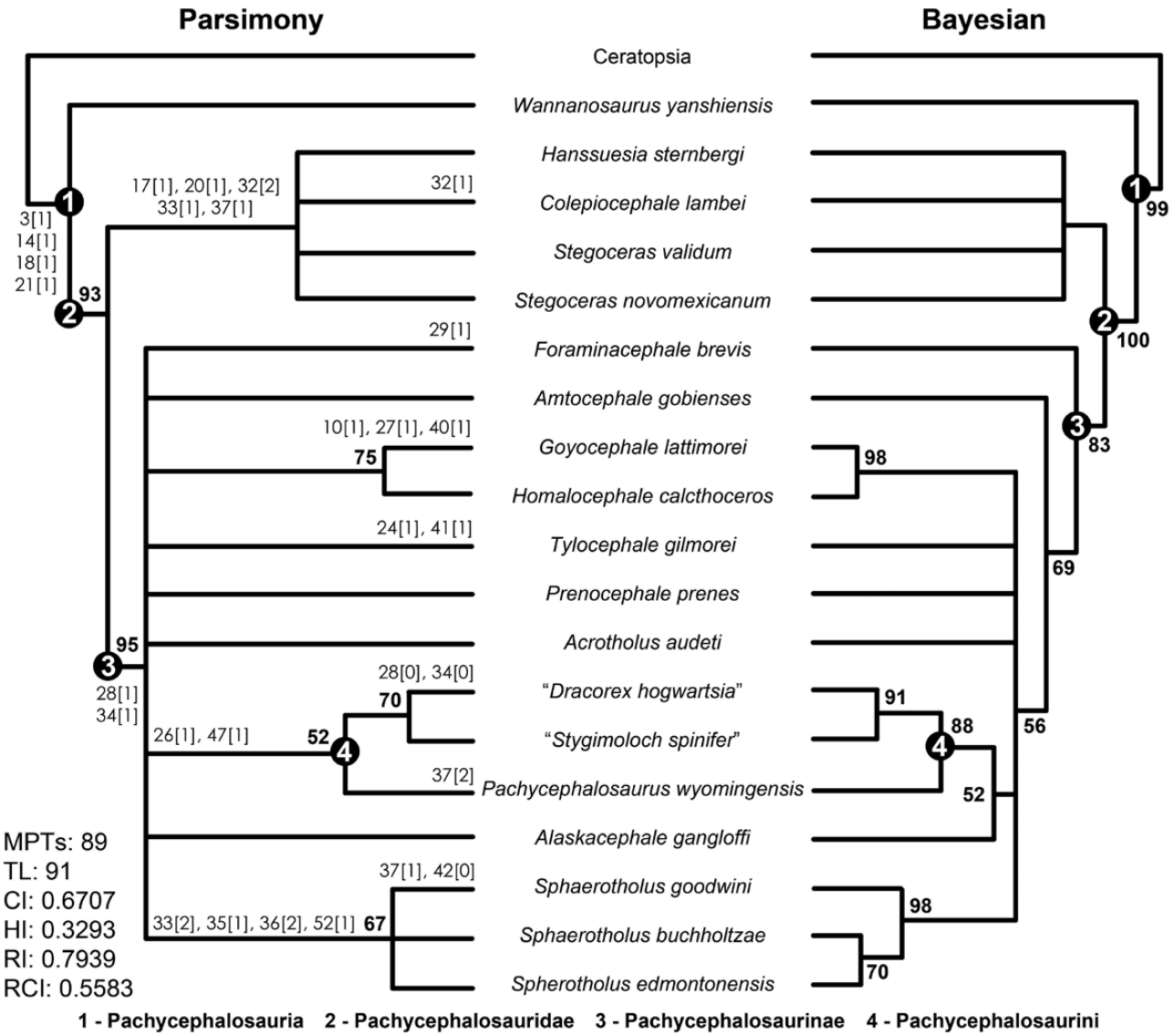

Figure 14. Phylogenetic analyses of *Pachycephalosauria* conducted during this study. Strict consensus parsimony analysis (left) compared to Bayesian analysis (right). Bold numbers in each analysis indicate clade credibility values; while the smaller numbers with brackets in the parsimony analysis correspond to synapomorphic/autapomorphic characters and states.

Longrich *et al.* (2010), Mallon *et al.* (2015), Schott & Evans (2016) and Williamson & Brusatte (2016), while *S. edmontonensis* is used by Sullivan (2000, 2003, 2005, 2006), Horner & Goodwin (2009), Schott *et al.* (2009), Longrich *et al.* (2010) and Mallon & Evans (2014). Even *S. buchholtzae* is not safe from misspellings, as it occurs erroneously as *S.* '*buchholtzi*' in Longrich *et al.* (2010). It is interesting that for nearly three decades, no consensus – or no taxonomic debate – surrounded the spelling of *S. edmontonensis* (although the taxonomy of the genus has been debated). It may seem a moot point, but what we call, and how we spell, the name of an organism is important. In some of the post-Sues & Galton (1987) works mentioned above, both spellings (*edmontonensis* and *edmontonense*) are used and often in context to genus referral or validity. However, we vehemently agree with and support how this matter was handled by Sullivan (2003). Opposed to tracking down the history, derivatives and merits of each spelling, Sullivan (2003) simply resorted back to *edmontonensis*, as this spelling has priority (Brown & Schlaikjer, 1943). This agrees with *Sphaerotholus*, which is a genus with a masculine gender, irrespective of the sex of the type specimen.

DISCUSSION

ONTOGENETIC AND HISTOLOGIC VARIATION IN *SPHAEROTHOLUS BUCHHOLTZAE*

As originally demonstrated in *Pachycephalosaurus* by Horner & Goodwin (2009), and later in *Stegoceras validum* (Schott *et al.*, 2011) and *Foraminacephale brevis* (Schott & Evans, 2016), void space (used as a proxy for vascularity) in pachycephalosaurid domes decreases through ontogeny. Although the spatial patterns and amount of void space amongst these taxa vary, all show a relatively consistent size-correlated trend of decreasing void space (i.e. vascularity). In *Stegoceras validum*, Schott *et al.* (2011) documented an ontogenetic decrease in vascular void space from approximately 20% to 7%, while in *Foramainacephale*, Schott & Evans (2016) documented the ontogenetic decrease from 1.67% to 0.25%. Unfortunately, the entire *Sphaerotholus buchholtzae* dataset described here could not be scanned to more finely test a hypothesized ontogenetic progression of vascularity, these representative smallest, intermediate and large domes indicate that vascularity in *Sphaerotholus* likewise decreased through ontogeny. The CT-based histological analysis conducted here suggested that UCMP 186026 is the least mature (21.3% vascularity), UWBM 98701 of intermediate maturity (11.4% vascularity) and DMNH EPV.97077 the most mature (2.5% vascularity). Histology, therefore, corroborates the hypothesis that size variation in the global sample can be interpreted to represent a growth series for this taxon. We, therefore, summarize the morphological changes and variation during growth below, both quantitatively and qualitatively.

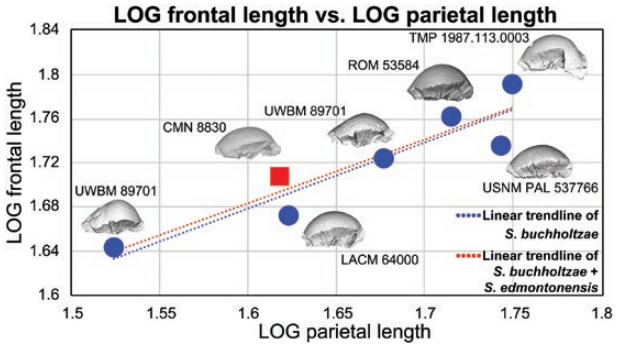

Figure 15. LOG frontal to parietal lengths in *Sphaerotholus buchholtzae* and *S. edmontonensis*. Note that the 'autapomorphic' condition of longer frontal to parietals as identified by Longrich *et al.* (2010) is not a legitimate observation once immature *S. buchholtzae* are included into the comparison. Left lateral orientations of each specimen not to scale.

Within the *Sphaerotholus* specimens examined in this analysis, we note a somewhat surprising degree of morphological variation, which was easily captured in morphometric analyses. Intraspecific variation can be problematic to assess in Dinosauria, particularly when only a single specimen is known for a given taxon and there is no way to know if that specimen conforms to the species norm. Even when numerous specimens are known, the disparity can be so dramatic that it may initially seem outside the scope of individual variation (such as the previously high diversity in Lambeosaurines: Dodson, 1975, Evans *et al*, 2005; Ryan & Evans, 2005; Evans, 2010; and *Triceratops* Marsh, 1889 species; Horner & Goodwin, 2006) and has been documented in other pachycephalosaurids, such as *Pachycephalosaurus* (Horner & Goodwin, 2009) and *Stegoceras* (Schott *et al.*, 2011). This is not the case here, since the size range and degree of variation exhibited by the sample *S. buchholtzae* is not extreme, but, nevertheless, its analysis is valuable for understanding pachycephalosaurid growth, ornamentation and systematics.

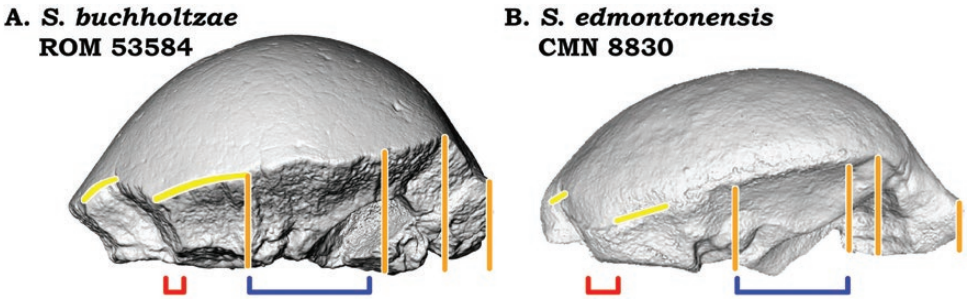

Figure 16. Potential morphologies to differentiate between *Sphaerotholus buchholtzae* and *S. edmontonensis*. Note the shorter anterior supraorbital (red) and longer postorbital length (blue) of *S. buchholtzae – the* opposite conditions in *S. edmontonensis*, the dorsoventrally taller posterior peripherial element contacts (orange) of *S. buchholtzae* to *S. edmontonensis,* and the more curved than straight dorsal margins of the anterior peripheral elements (yellow) of *S. buchholtzae* to *S. edmontonensis. Sphaerotholus buchholtzae* and *S. edmontonensis* are equal length in this image, but the actual specimens are not to scale.

Within the *Sphaerotholus buchholtzae* specimens examined herein, we hypothesize the following ontogenetic morphological changes in the skull roof based on the result from our morphometric analyses: smaller, immature individuals have an asymmetric dome curvature in lateral view in which the apex of the dome is more posteriorly located, opposed to a more symmetrically inflated dome in mature animals; smaller, immature animals have a more tesserate dome surface texture and more foramina exiting the dome than mature animals; immature individuals have a sharper posterior node row than the most mature animals. All of these trends have been noted in hypothesized ontogenetic series of *Stegoceras validum* (Williamson & Carr, 2002; Schott *et al.*, 2011; Schott & Evans, 2012), and some of these ontogenetic traits have been documented in *Foraminacephale* (Schott & Evans, 2016) and *Pachycephalosaurus* (Horner & Goodwin, 2009). We predict it is likely that they pertain to most, if not all, pachycephalosaurids.

As far as the variation in the frontoparietal is concerned, the length of the posterior portion of the parietals is either short or long; the posterior slope of the parietals is either relatively gradual (DMNH EPV.97077, USNM PAL 537766 and UWBM 89701) or steeper (ROM 53584, TMP 1987.113.0003 and UCMP 186026); the posteromedian process (intersquamosal process) of the parietal can be laterally wide (MOR 1605, ROM 53584) or relatively narrower (DMNH EPV.97077 and TMP 1987.113.0003); and domes appear to have either a high (LACM 64000 and ROM 53584) or low (MOR 3040 and USNM PAL 537766) lateral profile. Traditionally, some of these variable features, such as dome profile, were suggested to be sexual dimorphic (Chapman *et al.*, 1981; Sues & Galton, 1987). While sexual dimorphism does not need to be explicitly 50/50, we see no patterns in these variables that could be used to argue for sexual dimorphism. For instance, short posterior parietal processes are found on both high and low domes, as is dome height and posterior slope, or dome height and posterior process width. Furthermore, none of these variables are stratigraphically distinct (i.e. low domes low in formation, high domes higher up). Given the apparent randomness of these variables, we would conclude they reflect individual variation within the genus until larger, better constrained samples can be obtained.

Against the backdrop of this general ontogenetic bauplan, there is also considerable individual variation, particularly in the nodal ornamentation of the peripheral skull bones. As squamosal morphology and ornamentation represent a suite of highly important characters towards ontogeny and taxonomy (Williamson & Carr, 2002; Sullivan, 2003; 2005; 2006; Horner & Goodwin, 2009; Schott *et al.*, 2009; 2011; Longrich *et al.*, 2010; Evans *et al.*, 2011; Schott & Evans, 2012; 2016; Evans *et al.*, 2013; Mallon *et al.*, 2015; Goodwin & Evans, 2016), the understanding of *Sphaerotholus* squamosal morphology is, therefore, important for pachycephalosaurid systematics. Unfortunately, only a single specimen with squamosals is known for *S. goodwini* and no squamosals are yet known for *S. edmontonensis*, so assessments of squamosal variations must rely solely on those known from *S. buchholtzae*. Although all *S. buchholtzae* specimens have a single primary posterior node row and a lateral (postorbital–squamosal) row, the relative size and number of the individual nodes that form the parietosquamosal ornamentation is variable. While all specimens exhibit a lateroventral corner node, the proportional size of this node varies (a small corner node in TMP 1987.113.0003, to a larger node in ROM 75853); the primary node row can be constructed of either four (ROM 64809) or five (ROM 53582) nodes. In addition, it appears that the parietal portions of the medialmost parietosquamosal nodes are smaller in immature individuals than mature animals. Despite the variation noted above, the general pattern of ornamentation remains consistent across specimens and it maintains its diagnostic morphology over the size range of known specimens. Unfortunately, none of the squamosals appear to come from particularly small specimens, so our ontogenetic assessments of these characters is limited; but the general pattern of squamosal variation in *S. buchholtzae* is similar to *Stegoceras validum* (Schott & Evans, 2012), and this suggests that parietosquamosal variation provides valuable phylogenetic and taxonomic information in pachycephalosaurids.

In contrast to *S. buchholtzae*, in posterior view, the squamosal of *S. goodwini* exhibits a primary node row (constructed of five nodes) that has an extreme lateroventral pitch, as well as a ventrally located corner node that does not abut the node row. Compared to *Foraminacephale*, the primary node row count appears even more variable (four to seven) and, at least in comparable mature specimens, the squamosal bar is proportionally dorsoventrally taller (Schott & Evans, 2016). Finally, in comparison to *Prenocephale*, the node row number is comparable *S. buchholtzae* (five nodes). However, the nodes in *Prenocephale* decrease in size laterally, and nodes 1 and 5 do not abut nodes 2–4 (Evans *et al.*, 2018). Additionally. The corner node of *Prenocephale* does not abut the node row (as in *S. goodwini*).

At the genus level, Williamson & Carr (2002) noted in *Sphaerotholus*, that the posterior aspect of the parietal was laterally widened and incorporated two parietosquamosal nodes, and that such nodes are shared among *Sphaerotholus*, *Foraminacephale*, *Prenocephale* and *Tylocephale* (Williamson & Carr,

2002). Regarding the squamosal, and particularly its ornamentation, Williamson & Carr (2002) noted that the lateral corner node was reduced in size and situated above the ventral margin of the parietosquamosal bar; additionally, the nodes along the lateral margin of the parietosquamosal shelf were reduced on the squamosal and coalescing into a ridge on the postorbital (Williamson & Carr, 2002). The defining characters from the phylogenetic analyses of this study are supportive of the observations of Williamson & Carr (2002). While a parietosquamosal synapomorphy of *Sphaerotholus* is that the parietosquamosal bar shallows laterally (Character 36), this analysis phylogenetically also identified the parietosquamosal node (Character 42) as a synapomorphy.

Implications for pachycephalosaurine systematics

Perhaps the greatest topic of uncertainty in the literature regarding *Sphaerotholus* concerns its systematics and taxonomy. When Williamson & Carr (2002) erected the genus *Sphaerotholus*, they named and recognized two valid species: *S. goodwini* and *S. buchholtzae*. They recognized that *S. edmontonensis* (= '*Troödon edmontonensis*' of Brown & Schlaikjer, 1943), from the Horseshoe Canyon Formation of Alberta, was closely related to their newly erected species from the Hell Creek Formation (the holotype that had been previously referred to this species; Giffin, 1989). But Williamson & Carr (2002) regarded *S. edmontonensis* as a *nomen dubium*, due to the lack of known squamosals and any diagnostic traits, which also hindered phylogenetic analyses. Sullivan (2003) disagreed, and considered *S. buchholtzae* a subjective junior synonym of '*Prenocephale*' *edmontonensis*. Subsequently, Longrich *et al.* (2010) recognized *S. edmontonensis* as belonging to the genus *Sphaerotholus*, and that is was distinct from *S. goodwini* on the basis that the parietals are posteriorly broad and bear a pair of nodes, and from *S. buchholtzae* by putatively longer parietals (Longrich *et al.*, 2010: 279). Mallon *et al.* (2015) also recognized *S. edmontonensis* as distinct based on a morphometric analysis of postorbitals, and emphasized that *S. buchholtzae* was restricted to the latest Cretaceous Hell Creek Formation, and *S. edmontonensis* to the geologically older Horseshoe Canyon Formation of Canada; a hypothesis this analysis agrees with.

In a review of *S. edmontonensis* taxonomy, Sullivan (2000) considered that *S. edmontonensis* and *Foraminacephale brevis* belonged to the genus *Prenocephale*. Regarding *S. edmontonensis*, Sullivan (2000) noted that the fully domed frontoparietal, similar dome profile, the linear row of squamosal nodes, the linear node row continuing laterally along the squamosals, angled squamosal node row, the 'down-turn' of the parietals, were also observed in *Prenocephale prenes*. While we agree with Sullivan on many of the morphological similarities among these taxa, many of these characters, such as the linear posterior and lateral node row, the contributing parietosquamosal nodes, the distinct corner node and the 'down-turned' parietals, are likewise observed in *Acrotholus*, *Amtocephale*, *Pachycephalosaurus* and *Tylocephale*, and are, thus, likely plesiomorphic traits of Pachycephalosaurinae. While some phylogenetic analyses suggest a close relationship between *Prenocephale* and *Tylocephale* (Williamson & Carr, 2002; Schott *et al.*, 2009; Longrich *et al.*, 2010), most pachycephalosaurid studies recover a clade of *Sphaerotholus* species as phylogenetically distinct from *Prenocephale* (Williamson & Carr, 2002; Schott *et al.*, 2009; Longrich *et al.*, 2010; Watabe *et al.*, 2011; Evans *et al.*, 2013; Schott & Evans, 2016). Our phylogenetic analyses suggest that traits identified by Sullivan as characterizing *Prenocephale* are, in fact, symplesiomophies within pachycephalosaurine pachycephalosaurs, as opposed to being synapomorphies of a *Prenocephale* clade that includes the aforementioned taxa.

The new *Sphaerotholus buchholtzae* specimens described here provide a framework within which the debated taxonomic validity of *S. edmontonensis* can be evaluated. Only three specimens of *S. edmontonensis* have been found to-date and all of the specimens are incomplete and weathered domes, making it the least known of the *Sphaerotholus* species. The holotype (CMN 8830) is taphonomically modified (a high degree of rounding), therefore its precise morphologies are difficult to discern. Longrich *et al.* (2010) proposed that *S. edmontonensis* could be distinguished from *S. buchholtzae* by the proportionally anteroposteriorly longer parietals. Compared to larger, more mature *S. buchholtzae* specimens (like ROM 53584), the parietals of *S. edmontonensis* (CMN 8830) are indeed longer than the frontals. However, when compared to the *S. buchholtzae* ontogenetic series, this distinctive attribute disappears due to allometric growth (Fig. 15). Comparing LOG values of the frontal and parietal lengths, *S. edmontonensis* does not differ significantly from immature *S. buchholtzae*. Therefore, we agree that *S. edmontonensis* is distinct from *S. buchholtzae* (*sensu* Longrich *et al.*, 2010), but our analyses do not support 'longer parietals' as an autapomorphy of *S. edmontonensis*, as suggested by Longrich *et al.* (2010).

Unfortunately, peripheral elements that preserve potentially diagnostic ornamentation are currently unknown from *S. edmontonensis*. Therefore, only dome attributes and sutural contact morphologies can be used to test the distinctiveness of this species. The linear bivariate plots corroborate the results of Mallon *et al.*

(2015) with respect to the postorbital:frontoparietal proportions. Even with a scaled dome length, *S. edmontonensis* possesses a postorbital that is longer than any other *S. buchholtzae* in the linear analysis [40.4 mm vs. 25.56 and 36.15 mm (smallest and largest *S. buchholtzae* respectively)].

According to our morphometric analyses, two sutural contact geometrically set *S. edmontonensis* apart from *S. buchholtzae* – *the* sutural contacts for the postorbital (as linearly recognized) and that of the anterior supraorbital. Just as Mallon *et al.* (2015) recognized the postorbital proportional differences, the anteroposterior length of the anterior supraorbital is longer than that of *S. buchholtzae* [11.6 mm vs. 5.24 mm and 10.69 mm (smallest and largest *S. buchholtzae* respectively)]. Additionally, the profile of the peripheral elements may be used as a distinguishing trait. In all *S. buchholtzae* specimens equal to or larger than CMN 8830 in size, the sutures for the posterior peripheral elements are situated dorsally higher, and the anterior peripheral elements slope more ventrally. In CMN 8830 (and CMN 8831, which is missing the anteriormost region of the dome), the area of the anterior and posterior peripheral contacts are subequal, which produces a convex, as opposed to slanted, sutural profile (Fig. 16).

Unfortunately, we were not able to CT scan CMN 8830 in order to assess the relative maturity based on dome tissue composition, as has been done in other studies (Horner &Godwin, 2009; Schott *et al.*, 2011; Evans *et al.*, 2013; Schott & Evans, 2016). The relative size of CMN 8830 is approximate to the demonstrably immature *S. buchholtzae*, yet the rounded dome and rounded parietosquamosal nodes are both morphologies expressed in more mature individuals of *S. buchholtzae*. Additionally, there is no indication of tesserate surface texture in CMN 8830, which characterizes immature specimens of other pachycephalosaurids (Schott *et al.*, 2009; Schott *et al.*, 2011; Schott & Evans, 2016). Interestingly, many of the peripheral element sutural contacts, the convexed peripheral profile and the rectangular posterior parietal process, are all morphologies more akin to those in subadult-sized specimens of *S. buchholtzae* (such as LACM 64000, MOR 2926 and UWBM 89701). Yet, with the material at hand, it could be hypothesized that CMN 8830 represents a mature individual and that *S. edmontonensis* attained a smaller average body size than the later occurring *S. buchholtzae*.

Our biostratigraphic and morphometric results confirm, as noted by Mallon *et al.* (2015), that *Sphaerotholus buchholtzae* was found only within the Lancian-aged Hell Creek Formation and its equivalents (including the Frenchman Formation of Saskatchewan), and that *S. edmontonensis* was singularly restricted to the geologically older Horseshoe Canyon Formation of Canada. Together, the stratigraphy, phylogeny and morphology of the *Sphaerotholus* species present an interesting evolutionary hypothesis. As mentioned previously, all three species are temporally separated: *S. goodwini* (73.83 ± 0.18–73.49 ± 0.25 Mya; Fowler, 2017); *S. edmontonensis* (~68.4–70.9 Mya; Eberth *et al.*, 2013; Mallon *et al.*, 2015; Fowler, 2017); *S. buchholtzae* (~67.2–66.9 ± 0.2 Mya; Williamson & Carr, 2002; Mallon *et al.*, 2015; Fowler, 2017). The phylogenetic analyses, particularly the Bayesian analysis, finds *S. edmontonensis* and *S. buchholtzae* as sister-taxa. Additionally, the maturational assessment of the *S. buchholtzae* dataset morphologically supports *S. edmontonensis* (CMN 8830) as being mature. Seemingly contradictory though, the linear bivariate plots have *S. edmontonensis* always associating with immature *S. buchholtzae*. The fact that *S. edmontonensis* occurs immediately prior to its sister-taxon *S. buchholtzae*, and that the immature *S. buchholtzae* have close morphologic similarities with *S. edmontonensis* to the exclusion of other known species, are suggestive of an ancestor–descent relationship between the two taxa (Rozhdestvensky, 1965). While a thorough maturity assessment of *S. edmontonensis* must be conducted, the available data on the stratigraphy, relative ontogenetic maturity and morphologies similarly expressed in immature derived taxa, we tentatively hypothesize that *S. edmontonensis* and *S. buchholtzae* represent an anagenetic lineage within a single genus, and that both should be recognized as chronospecies.

Hell Creek Formation diversity

The diversity of the Hell Creek Formation dinosaur fauna has been the topic of a surge of recent research (Williamson & Carr, 2002; Carr & Williamson, 2004; Horner & Goodwin, 2006; Horner & Goodwin, 2009; Scannella & Horner, 2010; Campione & Evans, 2011; Horner *et al.*, 2011; Scannella *et al.*, 2014; Goodwin & Evans, 2016; Fowler, 2017). The ontogeny and diversity of small-bodied taxa like *Sphaerotholus*, has proven difficult to study, likely due in large part to scant remains related to taphonomic biases (e.g. Brown *et al.*, 2013). In terms of Hell Creek Formation pachycephalosaurid diversity, *Pachycephalosaurus* and its potential ontogimorphs have been the focus of most recent systematics' research (Goodwin & Horner, 2004; Bakker *et al.*, 2006; Snively & Cox, 2008; Horner & Goodwin, 2009; Williamson *et al.*, 2009; Peterson & Vittore, 2012; Peterson *et al.*, 2013, Goodwin & Evans, 2016), with little discussion of *Sphaerotholus* beyond taxonomic assessments based primarily on the type material.

Our analysis of a large sample of undescribed material from the Hell Creek Formation shows that *S. buchholtzae* is a distinct and valid taxon. *Sphaerotholus buchholtzae* is well represented by over 20 specimens.

Analysis of ontogeny and variation in the sample of *S. buchholtzae* exhibiting species-specific ornamentation provide a baseline for evaluating other named species of pachycephalosaurid, notably *S. edmontonensis*. Preliminary assessment of biostratigraphic variation in the sample reveals no recognizable directional patterns in morphology. We, therefore, hypothesize evolutionary stasis in dome shape and parietosquamosal traits through the Hell Creek section. However, based on the close relationships, morphological similarities and temporal distribution, *S. edmontonensis* may be the anagenetic ancestor of *S. buchholtzae*.

Analysis of dome histology in *S. buchholtzae*, using high resolution microCT scanning, and comparisons to other pachycepalosaurids, demonstrate that the largest of the known specimens have reached, or are approaching, skeletal maturity. Although complete specimens are not known, with a frontoparietal dome length of 116.3 mm (UALVP2), *Stegoceras validum* is reconstructed with a body length up to 2.5 m, and *Prenocephale* (ZPAL MgD-I/104) with a 143 mm dome at a similar body length (Sullivan, 2006). Although based on an undescribed postcranium ('Sandy'), *Pachycephalosaurus* replica mounts are reconstructed with a body length of 4.9 m. Assuming relative dome-to-body length isometry, *S. buchholtzae* would have been ~1.4–2.4 m long. Furthermore, assuming frontoparietal:femur proportions, *S. validum* (UALVP2) had a femur 222 mm long (Gilmore, 1924) and a minimum femoral circumference of 68 mm (Evans *et al.*, 2011), which results in a hypothetical femur length for *S. buchholtzae* (ROM 53584) as 213.31 mm and a minimum femoral circumference of 65.28 mm. These femoral proportions in *S. validum* (UALVP2) result in a calculated body mass of 16.9 kg (Campione *et al.*, 2014). With the dome of *S. buchholtzae* (ROM 53584) being approximately 96% the size of *S. validum* (UALVP2), dome:body mass isometry results in an estimated body mass of ROM 53584 of 16.2 kg. Within the Hell Creek Formation, *Pachycephalosaurus* is without doubt the larger of the two genera – frontoparietal dome length ~377 mm in AMNH FARB 1696 vs. ~112 mm in ROM 53584), and suggests that pachycephalosaurids in the Hell Creek ecosystems may have partitioned niches, at least in part, by body size. Even though *S. buchholtzae* physically represents a smaller component of the Hell Creek Formation biota, its presence within the formation means that pachycephalosaurid diversity during this critical interval, immediately before the end-Cretaceous extinction event, was higher than generally perceived.

Morphometric considerations

Within dinosaur palaeobiology, Hedrick & Dodson (2013) advocated, based on their 3D geometric study of *Psittacosaurus* skulls, that 2D GM is not well suited for skulls due to the spatial complexities [also echoed by Zelditch *et al.* (2012) for vertebrates and Van der Niet *et al.* (2010) for angiosperms, and others]. 2D GM is certainly the simpler and more straightforward of the two in terms of data acquisition and analysis. But a 2D analysis of complex 3D objects is not optimal, as 2D GM is most suitable for specimens that have most morphological variation within a single or restricted plane – such as footprints (Azevedo & Faria dos Santos, 2004; Castanera *et al.*, 2015), flat elements (Fearon & Varricchio, 2015), certain invertebrates (Sheets *et al.*, 2004; Glasby & Glasby, 2006; Bose *et al.*, 2011; Sasakawa 2016) and leaves (Shipunov & Bateman, 2005; Viscisi *et al.*, 2009; Viscosi & Cardini, 2011). However, the merits of 2D vs. 3D approaches are frequently discussed relative to specific morphological questions and taxonomic problems. In an examination of marmot dentaries, Cardini (2014) advocated for 3D GM, but found a negligible difference between 2D and 3D approaches. Furthermore, in their analysis of over 2000 avian skulls, Cooney *et al.* (2017) found nearly identical bill morphospace associations between 2D and 3D. Thus, these analyses appear to suggest that 2D and 3D approaches can both perform well for answering a suite of evolutionary questions where either dimensionality was sufficient to capture the most important aspects of shape variation. However, a recent analysis by Buser *et al.* (2017), which examined the relationship between mouth size and feeding ecology in sculpin fish, specifically tested the efficacy of 2D and 3D GM. They found that, while a 2D analysis did provide a general window into shape variations, it breaks down at fine scales. Additionally, 2D becomes imprecise when dealing with great morphologic variation, particularly with regards to the z-dimension (Buser *et al.*, 2017). In short, preforming a 2D analysis of a highly 3D object forces discrete spatial points into inaccurate locations.

The cranial domes of *Sphaerotholus* and other pachycephalosaurids are three-dimensional and have relatively subtle differences between taxa, making maximization of dimensional information vital. For example, looking at the position of the apex of the dome, while this point is not necessarily homologous, it is important because the anteroposterior location differs between taxa and changes ontogenetically. In immature *S. buchholtzae*, like UCMP 186026, the dome apex is posteriorly situated, while in mature *S. buchholtzae* (such as ROM 53584) it is more mid-length. This positioning may appear minor, but what of the dome apex in relation to the peripheral elements? In 2D this relationship would only appear to vary anteroposteriorly, but the dome is becoming circumferentially inflated, so through ontogeny the

distance between these points increases; a relationship that a lateral view 2D analysis does not adequately capture. One could certainly preform 2D GM in the six anatomical planes and compare the results, but at what point would such an approach be favourable to a single 3D analysis? With photogrammetry it has become relatively easy to produce accurate 3D models in vertebrate palaeobiology (Mallison & Wings, 2014); plus the numerous free programs to landmark and analyse, 3D GM is now almost as simple to conduct as 2D and it is preferable for complex 3D shapes like skulls, including the pachycephalosaurid domes analysed here.

In regard to the *Sphaerotholus* GM analysis, 2D and 3D do have agreeable trends or patterns. In both methodologies, all three species of *Sphaerotholus* do not morphospatially overlap in PC 1. Likewise, both methodologies find a morphospatial overlap between *S. buchholtzae* and *Foraminacephale* in PC 1 and 2. However, the finer nuances and more critical details greatly differ between 2D and 3D. Lateral 2D has no overlap between all three species of *Sphaerotholus* in PC 1 or 2. But the dorsal analysis has PC 2 overlap between *S. buchholtzae* and *S. edmontonensis*. It is also important to remember how these different orientations/analyses are testing the data. Both lateral and dorsal analyses highlighted the importance of the peripheral element sutural margins. In lateral view, the anteroposterior lengths and the dorsoventral heights of these contacts mattered; while in dorsal view, the emphasis was on the lateral width of points. The same landmark might be significant in both orientation analyses, but how they are interpreted from the question asked (i.e. orientation) is what differs. Alternatively, the 3D analysis examines the spatial relationships of these significant landmarks, but irrespective of the orientation. To reiterate, if the goal of the analysis to collect as much accurate spatial data as possible, why not collect and perform said analyses with a methodology that most effectively captures said spatial data?

CONCLUSION

This study of the pachycephalosaurine *Sphaerotholus* contributes toward an increased resolution of this marginocephalian clade. Ontogenetic series substantiate that pachycephalosaurs underwent extreme ontogenetic trajectories, as demonstrated by *Colepiocephale* (Schott *et al.*, 2009), *Foraminacephale* (Schott & Evans, 2016), *Pachycephalosaurus* (Horner & Goodwin, 2009), *Prenocephale* (Evans *et al.*, 2017), *Stegoceras* (Schott *et al.*, 2011) and now *Sphaerotholus buchholtzae*. *Sphaerotholus buchholtzae* exhibits the characteristic doming of the frontoparietal, loss of tessered surface texture, rounding or blunting of the squamosal nodes and decreased dome vascularity throughout ontogeny.

The broad stratigraphic range of *S. buchholtzae* through most of the Hell Creek Formation clearly demonstrates that the Hell Creek Formation, harboured at least two contemporaneous genera of pachycephalosaurids (regardless of the *Pachycephalosaurus* ontogimorph hypothesis; Horner & Goodwin, 2009), each of markedly different body size. As shown in preceding North American formations (e.g. Schott & Evans, 2016) and in Asia (e.g. Evans *et al.*, 2018), pachycephalosaurs exhibit a surprising degree of diversity, therefore a single genus within a formation (such as *S. edmontonensis* within the Horseshoe Canyon Formation) could be more anomalous.

In addition to documenting more about the life history of *S. buchholtzae*, this analysis also performed the first 3D GM analysis of pachycephalosaurid domes. As the frontoparietal represents a complex 3D structure, more traditional bivariate plots and standard 2D GM are not adequate techniques to encapsulate or reflect these shapes. The 3D GM analysis herein finds taxonomic support for the debated *Sphaerotholus* species *S. edmontonensis*, but it also shows the potential for taxonomic and ontogenetic assessments of other taxa.

ACKNOWLEDGEMENTS

We thank J. Scannella and the Museum of the Rockies, K. Seymour and the Royal Ontario Museum, J. Mallon and K. Shepherd of the Canadian Museum of Nature, G. Wilson, M. Rivin and the Burke Museum of Natural History and Culture, C. Mehling and the American Museum of Natural History, M. Walsh and the Natural History Museum of Los Angeles County, B. Strilisky of the Royal Tyrrell Museum, G. Liggett and the Bureau of Land Management, and R. Giesler and Paleo X for providing specimen access and information. T. Carr, R. Sullivan, J. Horner, R. Schott and T. Williamson provided valuable discussions and information regarding *Sphaerotholus*. T. Cullen, T. Lowi-Merri, K. Chiba, D. Jackson and B. Hedrick provided guidance, instruction and discussion on all things geometric morphometric related. The MOR *S. buchholtzae* specimens were collected on BLM and USFW lands. In addition to several specimens being collected from public lands today, many of the *S. buchholtzae* specimens included in this analysis were collected from indigenous lands of the Assiniboine, Crow and Gros Ventre tribes. Funding for this project was provided by Natural Science and Engineering Research Council of Canada (NSERC) Discovery Grant to DCE (NSERC Grant File Number:

RGPIN-2018–06788), a National Science Foundation (NSF) grant to MBG and DCE [NSF: EAR-1053370 to MBG; EAR-1561622 to High-Resolution X-ray Computed Tomography Facility, University of Texas at Austin (UTCT)]. M. Christenhusz, N. Fraser, J. Scannella and R. Sullivan provided valued, insightful and greatly appreciated revisions on earlier drafts of this manuscript. Finally, several Royal Ontario Museum peer review grants allowed a number of these specimens to be brought into the public trust. This manuscript represents contribution no. 1 to DCW's dissertation at the University of Toronto.

REFERENCES

Abramoff MD, **Magalhaes PJ**, **Ram SJ. 2004.** Image processing with ImageJ. *Biophotonics International* **11:** 36–42.

Adams DC, **Otárola-Castillo E. 2013.** Geomorph: an R package for the collection and analysis of geometric morphometric shape data. *Methods in Ecology and Evolution* **4:** 393–399.

Azevedo Rodrigues L, **Faria dos Santos V. 2004.** Sauropod tracks–a geometric morphometric study. In: Elewa AMT, ed. *Morphometrics: applications in biology and palaeontology*. Berlin and Heidelberg: Springer, 129–143.

Bakker RT, **Sullivan RM**, **Porter V**, **Larson P**, **Saulsbury SJ. 2006.** *Dracorex hogwartsia*, n. gen., n. sp., a spiked, flat-headed pachycephalosaurid dinosaur from the Upper Cretaceous Hell Creek Formation of South Dakota. *New Mexico Museum of Natural History and Science Bulletin* **35:** 331–345.

Bhullar BAS, **Marugán-Lobón J**, **Racimo F**, **Bever GS**, **Rowe TB**, **Norell MA**, **Abzhanov A. 2012.** Birds have paedomorphic dinosaur skulls. *Nature* **487:** 223.

Bose R, **Schneider CL**, **Leighton LR**, **Polly PD. 2011.** Influence of atrypid morphological shape on Devonian episkeletobiont assemblages from the lower Genshaw formation of the Traverse Group of Michigan: a geometric morphometric approach. *Palaeogeography, Palaeoclimatology, Palaeoecology* **310:** 427–441.

Bourke JM, **Ruger PWM**, **Ridgely RC**, **Lyson TR**, **Schachner ER**, **Bell PR**, **Witmer LM. 2014.** Breathing life into dinosaurs: tackling challenges of soft-tissue restoration and nasal airflow in extinct species. *The Anatomical Record* **297:** 2148–2186.

Brooks DR, **Bilewitch J**, **Condy C**, **Evans DC**, **Folinsbee KE**, **Fröbisch J**, **Halas D**, **Hill S**, **McLennan DA**, **Mattern M**, **Tsuji LA. 2007.** Quantitative phylogenetic analysis in the 21st century. Análisis filogenéticos cuantitativoa en el siglo XXI. *Revista Mexicana de Biodiversidad* **78:** 225–252.

Brown B, **Schlaikjer M. 1943.** A study of the troodont dinosaurs with the description of a new genus and four new species. *Bulletin of the AMNH* **82:** article 5.

Brown CM, **Evans DC**, **Ryan MJ**, **Russell AP. 2013.** New data on the diversity and abundance of small-bodied ornithopods (Dinosauria, Ornithischia) from the Belly River Group (Campanian) of Alberta. *Journal of Vertebrate Paleontology* **33:** 495–520.

Buser TJ, **Sidlauskas BL**, **Summers AP. 2017.** 2D or not 2D? Testing the utility of 2D vs 3D landmark data in geometric morphometrics of the sculpin subfamily Oligocottinae (Pisces; Cottoidea). *The Anatomical Record* **301:** 806–818.

Campione NE, **Evans DC. 2011.** Cranial growth and variation in edmontosaurs (Dinosauria: Hadrosauridae): implications for latest Cretaceous megaherbivore diversity in North America. *PLoS One* **6:** e25186.

Campione NE, **Evans DC**, **Brown CM**, **Carrano MT. 2014.** Body mass estimation in non-avian bipeds using a theoretical conversion to quadruped stylopodial proportions. *Methods in Ecology and Evolution* **5:** 913–923.

Carr TD, **Williamson TE. 2004.** Diversity of late Maastrichtian Tyrannosauridae (Dinosauria: Theropoda) from western North America. *Zoological Journal of the Linnean Society* **142:** 479–523.

Castanera D, **Colmenar J**, **Sauqué V**, **Canudo JI. 2015.** Geometric morphometric analysis applied to theropod tracks from the Lower Cretaceous (Berriasian) of Spain. *Palaeontology* **58:** 183–200.

Chapman RE, **Galton PM**, **Sepkoski JJ Jr**, **Wall WP. 1981.** A morphometric study of the cranium of the pachycephalosaurid dinosaur *Stegoceras*. *Journal of Paleontology* **55:** 608–618.

Cooney CR, **Bright JA**, **Capp E**, **Chira AM**, **Hughes EC**, **Moody CJA**, **Nouri LO**, **Varley ZK**, **Thomas GH. 2017.** Mega-evolutionary dynamics of the adaptive radiation of birds. *Nature* **542:** 344–347.

Dodson P. 1975. Functional and ecological significance of relative growth in Alligator. *Journal of Zoology* **175:** 315–355.

Eberth DA, **Evans DC**, **Brinkman DB**, **Therrien F**, **Tanke DH**, **Russell LS. 2013.** Dinosaur biostratigraphy of the Edmonton Group (Upper Cretaceous), Alberta, Canada: evidence for climate influence. *Canadian Journal of Earth Sciences* **50:** 701–726.

Evans DC, **Forster CA**, **Reisz RR. 2005.** The type specimen of *Tetragonosaurus erectofrons* (Ornithischia: Hadrosauridae) and the identification of juvenile lambeosaurines. In: Currie PJ, Koppelhus EB, eds. *Dinosaur Provincial Park, a spectacular ancient ecosystem revealed*. Bloomington: Indiana University Press, 349–366.

Evans DC, **Brown CM**, **Ryan MJ**, **Tsogtbaatar K. 2011.** Cranial ornamentation and ontogenetic status of *Homalocephale calathocercos* (Ornithischia: Pachycephalosauria) from the Nemegt Formation, Mongolia. *Journal of Vertebrate Paleontology* **31:** 84–92.

Evans DC, **Larson DW**, **Currie PJ. 2013.** A new dromaeosaurid (Dinosauria: Theropoda) with Asian affinities from the latest Cretaceous of North America. *Naturwissenschaften* **100:** 1041–1049.

Evans DC, **Hayashi S**, **Chiba K**, **Watabe M**, **Ryan MJ**, **Lee YN**, **Currie PJ**, **Tsogtbaatar K**, **Barsbold R. 2018.** Morphology and histology of new cranial specimens of Pachycephalosauridae (Dinosauria: Ornithischia) from

the Nemegt Formation, Mongolia. *Palaeogeography, Palaeoclimatology, Palaeoecology* **494:** 121–134.

Falkingham PL. 2012. Acquisition of high resolution three-dimensional models using free, open-source, photogrammetric software. *Palaeontologia Electronica* **15:** 15.

Fearon JL, **Varricchio DJ. 2015.** Morphometric analysis of the forelimb and pectoral girdle of the Cretaceous ornithopod dinosaur *Oryctodromeus cubicularis* and implications for digging. *Journal of Vertebrate Paleontology* **35:** e936555.

Fowler DW. 2017. Revised geochronology, correlation, and dinosaur stratigraphic ranges of the Santonian–Maastrichtian (Late Cretaceous) formations of the Western Interior of North America. *PLoS One* **12:** e0188426. Doi: 10.1371/journal.pone.0188426.

Giffin EB. 1989. Notes on pachycephalosaurs (Ornithischia). *Journal of Paleontology* **63:** 525–529.

Gilmore CW. 1931. A new species of troödont dinosaur from the Lance Formation of Wyoming. *Proceedings of the United States National Museum* **61:** 1–5.

Glasby CJ, **Glasby TM. 2006.** Two types of uncini in *Polycirrus* (Polychaeta: Terebellidae: Polycirrinae) revealed using geometric morphometrics. *Journal of Natural History* **40:** 237–253.

Goodwin MB. 1990. Morphometric landmarks of pachycephalosaurid cranial material from the Judith River Formation of northcentral Montana. In: Carpenter K, Currie PJ, eds. *Dinosaur systematics: perspectives and approaches*. London: Cambridge University Press, 189–201.

Goodwin MB, **Evans DC. 2016.** The early expression of squamosal horns and parietal ornamentation confirmed by new end-stage juvenile *Pachycephalosaurus* fossils from the Upper Cretaceous Hell Creek Formation, Montana. *Journal of Vertebrate Paleontology* **36:** e1078343.

Goodwin MB, **Horner JR. 2004.** Cranial histology of pachycephalosaurs (Ornithischia: Marginocephalia) reveals transitory structures inconsistent with head-butting behavior. *Paleobiology* **30:** 253–267.

Hedrick BP, **Dodson P. 2013.** Lujiatun psittacosaurids: understanding individual and taphonomic variation using 3D geometric morphometrics. *PLoS One* **8:** e69265.

Heled J, **Bouckaert RR. 2013.** Looking for trees in the forest: summary tree from posterior samples. *BMC Evolutionary Biology* **13:** 221.

Horner JR, **Goodwin MB. 2006.** Major cranial changes during *Triceratops* ontogeny. *Proceedings of the Royal Society of London B: Biological Sciences* **273:** 2757–2761.

Horner JR, **Goodwin MB. 2009.** Extreme cranial ontogeny in the Upper Cretaceous dinosaur *Pachycephalosaurus*. *PLoS One* **4:** e7626.

Horner JR, **Goodwin MB**, **Myhrvold N. 2011.** Dinosaur census reveals abundant *Tyrannosaurus* and rare ontogenetic stages in the Upper Cretaceous Hell Creek Formation (Maastrichtian), Montana, USA. *PLoS One* **6:** e16574.

Huang LK, **Wang MJJ. 1995.** Image thresholding by minimizing the measures of fuzziness. *Pattern Recognition* **28:** 41–51.

JMP. 1989–2020. *JMP, v.14.1.0*. Cary: SAS Institute Inc. Software Available at: https://www.jmp.com/en_us/software/data-analysis-software.html.

Kawabe S, **Matsuda S**, **Tsunekawa N**, **Endo H. 2015.** Ontogenetic shape change in the chicken brain: implications for paleontology. *PLoS One* **10:** e0129939.

Lambe LM. 1918. The Cretaceous genus *Stegoceras*, typifying a new family referred provisionally to the Stegosauria. *Transactions of the Royal Society of Canada* **12:** 23–36.

Lautenschlager S. Hübner T. 2013. Ontogenetic trajectories in the ornithischian endocranium. *Journal of Evolutionary Biology* **26:** 2044–2050.

Longrich NR, **Sankey J**, **Tanke D. 2010.** *Texacephale langstoni*, a new genus of pachycephalosaurid (Dinosauria: Ornithischia) from the upper Campanian Aguja Formation, southern Texas, USA. *Cretaceous Research* **31:** 274–284.

Mallison H, **Wings O. 2014.** Photogrammetry in paleontology – a practical guide. *Journal of Paleontological Techniques* **12:** 1–31.

Mallon JC, **Evans DC. 2014.** Taphonomy and habitat preference of North American pachycephalosaurids (Dinosauria, Ornithischia). *Lethaia* **47:** 567–578.

Mallon JC, **Evans DC**, **Tokaryk TT**, **Currie ML. 2015.** First pachycephalosaurid (Dinosauria: Ornithischia) from the Frenchman Formation (upper Maastrichtian) of Saskatchewan, Canada. *Cretaceous Research* **56:** 426–431.

Maryańska T, **Osmólska H. 1974.** Pachycephalosauria, a new suborder of ornithischian dinosaurs. *Palaeontologica Polonica* **30:** 45–102.

Maryańska T, **Chapman RE**, **Weishampel DB. 2004.** Pachycephalosauria. In: Weishampel DB, Dodson P, Osmólska H, eds. *The Dinosauria*, *2nd edn*. Berkeley: University of California Press, 464–477.

O'Reilly JE, **Puttick NM**, **Parry L**, **Tanner AR**, **Tarver JE**, **Fleming J**, **Pisani D**, **Donoghue PCJ. 2016.** Bayesian methods outperform parsimony but at the expense of precision in the estimation of phylogeny from discrete morphological data. *Biology Letters* **12:** 20160081.

Owen R. 1842. *Report on British fossil reptiles. Part II. Report of the Eleventh Meeting of the British Association for the Advancement of Science; Held at Plymouth in July 1841*. London: John Murray, 60–204.

Peterson JE, **Vittore CP. 2012.** Cranial pathologies in a specimen of *Pachycephalosaurus*. *PLoS One* **7:** e36227.

Peterson JE, **Dischler C**, **Longrich NR. 2013.** Distributions of cranial pathologies provide evidence for head-butting in dome-headed dinosaurs (Pachycephalosauridae). *PLoS One* **8:** e68620.

Puttick MN, **O'Reilly JE**, **Tanner AR**, **Fleming JF**, **Clark J**, **Holloway L**, **Lozano-Fernandez J**, **Parry LA**, **Tarver JE**, **Pisani D**, **Donoghue PC. 2017.** Uncertain-tree: discriminating among competing approaches to the phylogenetic analysis of phenotype data. *Proceedings of the Royal Society of London B: Biological Sciences* **284:** 20162290.

R Development Core Team. **2008.** *R: a language and environment for statistical computing*. Vienna: R Foundation for Statistical Computing. Available at: http://www.R-project.org.

Ronquist F, **Teslenko M**, **Van der Mark P**, **Ayres DL**, **Darling AD**, **Höhna S**, **Larget B**, **Liu L**, **Suchard MA**, **Huelsenbeck JP. 2012.** MrBayes 3.2: efficient Bayesian

phylogenetic inference and model choice across a large model space. *Systematic Biology* **61:** 539–542.

Rozhdestvensky AK. 1965. Growth changes in Asian dinosaurs and some problems of their taxonomy. *Paleontologičeskij Žurnal* **3:** 95–109.

Ryan MJ, **Evans DC. 2005.** Ornithischian dinosaurs. In: Currie PJ, Koppelhus EB, eds. *Dinosaur Provincial Park, a spectacular ancient ecosystem revealed*. Bloomington: Indiana University Press, 312.

Sasakawa K. 2016. Utility of geometric morphometrics for inferring feeding habit from mouthpart morphology in insects: tests with larval Carabidae (Insecta: Coleoptera). *Biological Journal of the Linnean Society* **118:** 394–409.

Scannella JB, **Horner JR. 2010.** *Torosaurus* Marsh, 1891, is *Triceratops* Marsh, 1889 (Ceratopsidae: Chasmosaurinae): synonymy through ontogeny. *Journal of Vertebrate Paleontology* **30:** 1157–1168.

Scannella JB, **Fowler DW**, **Goodwin MB**, **Horner JR. 2014.** Evolutionary trends in *Triceratops* from the Hell Creek Formation, Montana. *Proceedings of the National Academy of Sciences of the USA* **111:** 10245–10250.

Schott RK, **Evans DC. 2012.** Squamosal ontogeny and variation in the pachycephalosaurian dinosaur Stegoceras validum Lambe, 1902, from the Dinosaur Park Formation, Alberta. *Journal of Vertebrate Paleontology,* **32:** 903–913.

Schott RK, **Evans DC. 2016.** Cranial variation and systematics of *Foraminacephale brevis* gen. nov. and the diversity of pachycephalosaurid dinosaurs (Ornithischia: Cerapoda) in the Belly River Group of Alberta, Canada. *Zoological Journal of the Linnean Society* **179:** 865–906.

Schott RK, **Evans DC**, **Williamson TE**, **Carr TD**, **Goodwin MB. 2009.** The anatomy and systematics of *Colepiocephale lambei* (Dinosauria: Pachycephalosauridae). *Journal of Vertebrate Paleontology* **29:** 771–786.

Schott RK, **Evans DC**, **Goodwin MB**, **Horner JR**, **Brown CM**, **Longrich NR. 2011.** Cranial ontogeny in *Stegoceras validum* (Dinosauria: Pachycephalosauria): a quantitative model of pachycephalosaur dome growth and variation. *PLoS One* **6:** e21092.

Seeley HG. 1888. Classification of the Dinosauria. *Geological Magazine (Decade III)* **5:** 45–46.

Sereno PC. 1997. The origin and evolution of dinosaurs. *Annual Review of Earth and Planetary Sciences* **25:** 435–489.

Sereno PC. 1998. A rationale for phylogenetic definitions, with application to the higher-level taxonomy of Dinosauria. *New Yearbook for Geology and Paleontology Treatises* **210:** 41–83.

Sheets HD, **Kim K**, **Mitchell CE. 2004.** A combined landmark and outline-based approach to ontogenetic shape change in the Ordovician trilobite *Triarthrus becki*. In: Elewa AMT, ed. *Morphometrics, applications in biology and paleontology*. Berlin and Heidelberg: Springer, 67–82.

Shipunov AB, **Bateman RM. 2005.** Geometric morphometrics as a tool for understanding *Dactylorhiza* (Orchidaceae) diversity in European Russia. *Biological Journal of the Linnean Society* **85:** 1–12.

Snively E, **Cox A. 2008.** Structural mechanics of pachycephalosaur crania permitted head-butting behavior. *Palaeontologia Electronica* **11:** 3A.

Sternberg CM. 1945. Homalocephaloidae proposed for dome-headed dinosaurs, *Stegoceras lambei*, n. sp., described. *Journal of Paleontology* **19:** 534–538.

Sues HD, **Galton PM. 1987.** Anatomy and classification of the North American Pachycephalosauria (Dinosauria: Ornithischia). E. Schweizerbart'sche.

Sprain CJ, **Renne PR**, **Clemens WA**, **Wilson GP. 2018.** Calibration of chron C29r: New high-precision geochronologic and paleomagnetic constraints from the Hell Creek region, Montana. *Bulletin,* **130:** 1615–1644.

Sullivan RM. 2000. *Prenocephale edmontonensis* (Brown and Schlaikjer) new comb. and *P. brevis* (Lambe) new comb. (Dinosauria: Ornithischia: Pachycephalosauria) from the Upper Cretaceous of North America. *Dinosaurs of New Mexico: Bulletin* **17:** 177–190.

Sullivan RM. 2003. Revision of the dinosaur *Stegoceras* Lambe (Ornithischia, Pachycephalosauridae). *Journal of Vertebrate Paleontology* **23:** 181–207.

Sullivan RM. 2005. Pachycephalosaurs from Dinosaur Provincial Park, Alberta: taxonomy, biostratigraphy, and paleobiogeographic implications. In: *Dinosaur Park Symposium – short papers, abstracts, and program*. Drumheller: Special Publication of the Royal Tyrrell Museum, 121–126.

Sullivan RM. 2006. A taxonomic review of the Pachycephalosauridae (Dinosauria: Ornithischia). *New Mexico Museum of Natural History and Science Bulletin* **35:** 347–365.

Swofford DL. 2002. *PAUP*: phylogenetic analysis using parsimony (* and other methods)*. Sunderland: Sinauer.

Van der Niet T, **Zollikofer CP**, **de León MSP**, **Johnson SD**, **Linder HP. 2010.** Three-dimensional geometric morphometrics for studying floral shape variation. *Trends in Plant Science* **15:** 423–426.

Viscosi V, **Cardini A. 2011.** Leaf morphology, taxonomy and geometric morphometrics: a simplified protocol for beginners. *PLoS One* **6:** e25630.

Viscosi V, **Lepais O**, **Gerber S**, **Fortini P. 2009.** Leaf morphological analyses in four European oak species (Quercus) and their hybrids: a comparison of traditional and geometric morphometric methods. *Plant Biosystems* **143:** 564–574.

Wang Q, **Chi Z**, **Zhao R. 2002.** Image thresholding by maximizing the index of nonfuzziness of the 2-D grayscale histogram. *Computer Vision and Image Understanding* **85:** 100–116.

Watabe M, **Tsogtbaatar K**, **Sullivan RM. 2011.** A new pachycephalosaurid from the Baynshire Formation (Cenomanian–late Santonian), Gobi Desert, Mongolia. Fossil Record 3. *New Mexico Museum of Natural History and Science, Bulletin* **53:** 489–497.

Williamson TE, **Brusatte SL. 2016.** Pachycephalosaurs (Dinosauria: Ornithischia) from the Upper Cretaceous (upper Campanian) of New Mexico: a reassessment of *Stegoceras novomexicanum*. *Cretaceous Research* **62:** 29–43.

Williamson TE, **Carr TD. 2002.** A new genus of derived pachycephalosaurian from western North America. *Journal of Vertebrate Paleontology* **22:** 779–801.

Williamson TE, **Carr TD**, **Williams SA**, **Tremaine K. 2009.** Early ontogeny of pachycephalosaurine squamosals as revealed by juvenile specimens from the Hell Creek Formation, eastern Montana. *Journal of Vertebrate Paleontology* **29:** 291–294.

Wiley DF, **Amenta N**, **Alcantara DA**, **Ghosh D**, **Kil YJ**, **Delson E**, **Harcourt-Smith W**, **Rohlf FJ**, **St. John K**, **Hamann B. 2005.** Evolutionary morphing. In: *VIS 05. IEEE Visualization*. 431–438. Available at; https://ieeexplore.ieee.org/document/1532826.

Wilson GP, Clemens WA, Horner JR, Hartman JH, eds. 2014. *Through the end of the Cretaceous in the type locality of the Hell Creek Formation in Montana and adjacent areas*. Boulder: Geological Society of America (special paper 503).

Wright AM, **Hillis DM. 2014.** Bayesian analysis using a simple likelihood model outperforms parsimony for estimation of phylogeny from discrete morphological data. *PLoS One* **9:** e109210.

Zelditch ML, **Swiderski DL**, **Sheets HD. 2012.** *Geometric morphometrics for biologists: a primer*. Amsterdam: Elsevier.

SUPPORTING INFORMATION

Additional Supporting Information may be found in the online version of this article at the publisher's web-site.

Figure S1. Schematic of measurements taken on *Sphaertholus* specimens.

Figure S2. Photographs of the holotype of *Sphaerotholus buchholtzae* TMP 1987.113.0003 in right lateral (A), dorsal (B), ventral (C) and posterior (D) views. All orientations to scale. Scale bar = 2 cm. Please note that in MS Figures 1, 5, 8, 9, 13, TMP 1987.113.0003 is represented by either photographs of a cast or a photogrammetric model. At the time of personal examination, DCW did not get all of the angled orientation images, such as those used in Figure 5. The description of TMP 1987.113.0003 by Williamson & Carr (2002) likewise relied on examination of this cast (TEW pers. comm.); therefore, the use herein is applicable to the holotypic description. However, in the fall of 2020, attempts were made by the authors to acquire additional photographs. Unfortunately, due to the ongoing global pandemic, travel and museum access were not safely advisable. Though not a perfect substitute, we have provided a plate of the fossil of TMP 1987.113.0003 should readers like to compare the morphology of the cast to the actual specimen.

APPENDIX I

Character states and matrix used in the phylogenetic analysis. The characters list is based on Evans *et al.* (2013) and Schott & Evans (2016). New characters are denoted with (new) at the end.

1. Posterior sacral rib length: short and subrectangular (0); strap-shaped and elongate (1).
2. Preacetabular process, shape of distal end: tapered and subveritcally oriented (0); dorsoventrally flattened and expanded distally.
3. Humeral length: more (0), or less than (1), 50% of femoral length.
4. Humeral shaft form: straight (0); bowed (1).
5. Deltopectoral crest development: strong (0); rudimentary (1).
6. Zygapophyseal articulations, form: flat (0); grooved (1).
7. Ossified tendons: bundled, rodlike (0); caudal basket, fusiform (1).
8. Sternal shape: plate-shaped (0); shafted (1).
9. Iliac blade, lateral deflection of preacetabular process weak (0); marked (1).
10. Iliac blade, position of medial tab: absent (0); above acetabulum (1); on postacetabular process (2).
11. Postacetabular process of ilium: elongate and subrectangular (0); deep and downturned distally, with an arcuate dorsal margin (1).
12. Ischial pubic peduncle, shape: dorsoventrally (0), or transversely (1); flattened.
13. Pubic body: substantial (0); reduced, nearly excluded from acetabulum (1).
14. Frontal and parietal thickness: thin (0); thick (1).
15. Arched premaxilla-maxilla diastema: absent (0); present (1).
16. Postorbital-squamosal bar, form: strap-shaped with a narrow dorsal margin (0); broad, flattened (1).
17. Squamosal exposure on occiput: restricted (0); broad (1).
18. Supraorbital bones 1 and 2: absent (0); present, and exclude the frontal from the orbital rim (1).
19. Postorbital-jugal bar, position of descending process of postorbital: extends to the ventral margin of the orbit (0); terminates above the ventral margin of the orbit, interdigitate postorbital-jugal contact (1).
20. Parietal septum, form: narrow and smooth (0); broad and rugose, has dorsal ornamentation (1).
21. Infratemporal fenestra size: larger than orbit, lower temporal bar long (0); smaller than orbit, lower

AQ7AQ31

temporal bar greatly shortened, jugal and quadrate in close proximity or have a small contact (1).
22. Pterygoquadrate rami, posterior projection of ventral margin: weak, jaw joint at the approximate level of occusal surface (0); pronounced, jaw joint below occlusal surface (1).
23. Prootic-basisphenoid plate: absent (0); present (1).
24. Quadratojugal fossa: absent (0); present (1).
25. Quadrate, posterior ramus in lateral view: subvertical or gently curved dorsally (0); sinuous, quadrate strongly inclined dorsally, posterior ramus embayed (1).
26. Skull: relatively short, rostrum has a convex profile (0); relatively long, rostrum has a concave dorsal profile (1).
27. Epaxial muscle attachment scars on ventrocaudal margin of paroccipital process, caudal view: absent or indistinct (0); broad extending from ventrocaudal margin of paroccipital process and including region above foramen magnum (1); restricted to area dorsolateral to foramen magnum (2).
28. Supratemporal fenestra: open (0); closed (1).
29. Roof of temporal chamber as manifest on parietal in lateral view: absent (0); small, roof horizontal (1); enlarged, dorsally arched (2).
30. Grooves in frontal: absent (0); present (1).
31. Contact of anterior supraorbital with frontal: absent (0); restricted (1); extensive (2).
32. Doming of frontoparietal: absent (0); does not include supraorbital lobes (1); includes supraorbital lobes (2).
33. Dorsal margins of postorbital and posterior supraorbital sutural surfaces on dome: postorbital and supraorbital II do not form part of a dome (0); dorsally arched such that there is a distinct diastema between the two (1); both are straight and continuous, diastema absent (2).
34. Frontoparietal dome in lateral view, caudal margin of parietal dome blends with parietosquamosal shelf along a curve: absent (0); present (1).
35. Parietosquamosal bar in caudal view (viewed perpendicular to shelf): horizontal or slopes at a shallow ventrolateral angle (0); slopes at a steep ventrolateral angle (1).
36. Parietosquamosal bar beneath the primary node row: absent (0); maintains approximately the same depth or slightly deepens laterally (1); shallows laterally (2).
37. Exposure of posteromedian (intersquamosal) process between squamosals: caudolateral wings well developed (0); restricted (1); broad (2).
38. Extensive intersquamosal joint posterior to parietal: absent (0), present (1).
39. Parietosquamosal bar primary (enlarged) nodes: absent (0); in a single row (1); in two or more rows sometimes appearing clustered (2).
40. Number of nodes in the primary parietosquamosal node row: 5 or less (0) 6 or more (1).
41. Irregular tuberculate ornamentation on caudal surface of squamosal below the primary node row: absent (0); present (1).
42. A coalescing node with constituents on the parietal and squamosal (i.e. a parietosquamosal node): absent (0); present (1). (new)
43. Medialmost nodes in primary parietosquamosal node row, enlarged relative to all other nodes: absent (0); present (1).
44. Enlarged corner node on squamosal ventrolateral to primary node row of parietosquamosal bar: absent (0); present (1).
45. Secondary corner node, medial to the lateroventral corner node: absent (0); present (1).
46. Squamosal, several nodes drawn out into long spikes: absent (0); present (1).
47. Large, conical node projects laterally from jugal: absent (0); present (1).
48. Rostral nodes: absent (0); continue from the supraorbital shelf onto the dorsal region of the rostrum (1); cover the dorsal surface of rostrum and form series of 'half rings' (2).
49. Postorbital node row: absent (0); present (1).
50. Posterolateral edge of skull formed by squamosal and postorbital in dorsal view: straight (0); convex (1).
51. Posterior accessory node on squamosal ventral to nodes 3 and 4 in the primary parietosquamosal node row: absent (0); present (1). (new)

Character matrix:

Psittacosaurus mongolensis													
	0	0	0	0	0	0	0	0	0	0	0	0	0
	0	0	0	0	0	0	0	0	0	0	0	0	0
	0	0	0	0	0	0	0	0	0	0	0	0	0
	0	0	0	0	0	0	0	0	0	0	0	0	
Yinlong downsi													
	0	0	0	?	1	0	0	?	0	0	0	0	?
	0	0	1	0	0	1	0	0	0	?	?	0	0
	?	0	0	0	0	0	0	0	0	0	0	0	1
	0	0	0	0	0	0	0	0	0	0	0	0	
Wannanosaurus yanshiensis													
	?	?	1	1	0	?	?	?	?	?	?	?	?
	1	?	1	0	1	1	0	1	?	?	?	?	?
	?	0	?	?	?	0	0	0	0	?	0	0	1
	?	0	0	0	0	0	0	0	?	0	0	0	
Goyocephale lattimorei													
	1	1	1	1	1	1	1	1	1	1	0	?	?
	1	1	1	1	1	1	1	?	?	1	?	?	0
	1	0	?	0	1	0	0	0	0	1	2	0	1
	1	1	?	1	1	1	0	?	1	1	1	?	
Homalocephale calathocercos													
	1	1	?	?	?	1	1	1	1	2	1	0	1
	1	?	1	1	1	1	1	1	1	1	0	1	0
	2	0	?	0	?	0	0	0	0	1	2	0	1
	0	1	1	1	1	1	0	0	?	1	1	0	
Tylocephale gilmorei													
	?	?	?	?	?	?	?	?	?	?	?	?	?
	1	?	1	1	1	1	1	1	1	?	1	?	0
	2	1	?	0	?	2	1	?	0	1	?	0	1
	0	1	?	0	1	0	0	0	?	?	0	0	
Prenocephale prenes													
	1	1	?	?	1	1	1	?	1	2	1	0	1
	1	1	1	1	1	1	1	1	1	1	0	1	0
	2	1	?	0	1	2	1	1	0	1	1	0	1
	0	0	0	0	1	0	0	0	1	1	1	0	
Foraminacephale brevis													
	?	?	?	?	?	?	?	?	?	?	?	?	?
	1	?	1	1	1	?	1	?	?	?	?	?	?
	?	1	1	1	2	2	1	1	0	1	2	0	1
	1	0	1	0	1	0	0	?	?	0	1	0	
Hanssuesia sternbergi													
	?	?	?	?	?	?	?	?	?	?	?	?	?
	1	?	1	1	1	?	1	?	?	?	?	?	?
	?	0	1	1	2	2	1	?	?	?	?	?	?
	?	?	?	?	?	?	?	?	?	?	?	?	
Colepiocephale lambei													
	?	?	?	?	?	?	?	?	?	?	?	?	?
	1	?	?	?	1	?	?	?	?	?	?	?	?
	?	0/1	1	1	2	1	1	0	?	?	?	?	?
	?	?	?	?	?	?	?	?	?	?	?	?	
Stegoceras validum													
	?	1	1	1	1	1	1	1	0	2	0	1	1

	1	0	1	1	1	1	1	1	1	1	0	1	0
	1	0/1	1	1	2	2	1	0	0	1	1	0	1
	1	1	0/1	1	0	0	0	0	0	0	0	0	
Dracorex hogwartsia													
	?	?	?	?	?	1	?	?	?	?	?	?	?
	1	1	1	1	1	?	1	1	1	?	0	1	1
	1	0	?	0	?	0	0	0	0	?	1	1	2
	0	0	0	0	1	0	1	1	2	1	0	0	
Stygimoloch spinifer													
	?	?	?	?	?	?	1	?	?	?	?	?	?
	1	?	1	1	1	?	1	?	?	?	?	?	1
	?	1	2	0	1	1	?	1	0	?	1	1	2
	0	0	0	0	1	0	1	1	2	1	0	0	
Pachycephalosaurus wyomingensis													
	?	?	?	?	?	?	?	?	?	?	?	?	?
	1	?	1	1	1	1	1	1	1	?	0	1	1
	1	1	2	0	1	2	2	1	0	?	2	0	2
	0	0	?	0	1	0	0	1	2	1	0	0	
Alaskacephale gongloffi													
	?	?	?	?	?	?	?	?	?	?	?	?	?
	1	?	1	1	1	1	1	?	?	?	0	?	?
	?	1	2	0	?	?	?	1	?	1	?	0	2
	0	0	?	0	?	0	0	?	?	?	?	?	
Sphaerotholus goodwini													
	?	?	?	?	?	?	?	?	?	?	?	?	?
	1	?	1	1	1	1	1	?	?	1	?	?	?
	2	1	2	0	1	2	2	1	1	2	1	0	1
	0	0	0	0	1	0	0	?	?	0	1	?	
Sphaerotholus buchholtzae													
	?	?	?	?	?	?	?	?	?	?	?	?	?
	1	?	1	1	1	?	1	?	?	?	?	?	?
	?	1	2	0	1	2	2	1	1	2	2	0	1
	0	0	1	0	1	0	0	?	?	0	1	1	
Sphaerotholus edmontonensis													
	?	?	?	?	?	?	?	?	?	?	?	?	?
	1	?	?	1	?	?	?	?	?	?	?	?	?
	?	1	2	0	1	2	2	1	?	?	2	0	?
	?	?	1	?	?	?	?	?	?	?	1	?	
Acrotholus audeti													
	?	?	?	?	?	?	?	?	?	?	?	?	?
	1	?	1	1	1	?	1	?	?	?	?	?	?
	?	1	2	0	1	2	1	1	?	?	1	?	?
	?	?	0	?	?	?	?	?	?	?	?	?	
Stegoceras novomexicanum													
	?	?	?	?	?	?	?	?	?	?	?	?	?
	1	?	?	?	1	?	1	?	?	?	?	?	?
	?	0	1	1	2	2	1	0	?	?	1	0	?
	?	?	1	?	?	?	?	?	?	?	?	?	
Amtocephale gobienses													
	?	?	?	?	?	?	?	?	?	?	?	?	?
	1	?	?	?	1	?	1	?	?	?	?	?	?
	?	1	2	?	2	2	1	1	?	?	2	0	?
	?	?	?	?	?	?	?	?	?	?	?	?	